water

MDPI

Article

Hydrogeochemistry and Mercury Contamination of Surface Water in the Lom Gold Basin (East Cameroon): Water Quality Index, Multivariate Statistical Analysis and Spatial Interpolation

Marie Sorella Bella Atangana [1,2], Jules Rémy Ndam Ngoupayou [2] and Jean-François Deliege [1,*]

[1] PeGIRE Laboratory (Aquapole R&D Unit), Research Unit—FOCUS, Department of Biology, Ecology and Evolution (BEE), Faculty of Sciences, University of Liège, Aquapôle, Bat. B53 Campus Sart-Tilman, 4000 Liège, Belgium; aquapole@ulg.ac.be

[2] Hydrogeology Laboratory, Department of Earth Sciences, University of Yaoundé I, Rte de l'Université, Yaoundé 33088, Cameroon; jules-remy.ndam@facsciences-uy1.cm

* Correspondence: jfdeliege@uliege.be

Abstract: Artisanal and small-scale gold mining activities have an impact on natural resources and human health. This study addresses the assessment of surface water quality in the Lom gold basin. A combined approach of water quality index calculation, multivariate statistical analysis and spatial interpolation was used. Sampling was performed at 15 stations during low- and high-water periods in 2021 for classical physicochemical parameters and total mercury measurements. The results show that the physicochemical parameters were below drinking water standards for both periods, except for pH, total suspended solids and total mercury. These waters show a large cation deficit as well as an anion deficit. The water chemistry is controlled by precipitations and silicate dissolutions in rock that convert the water into the Ca-HCO_3 and Ca-Mg-HCO_3 types. The level of mercury contamination varied from acceptable to high due to high flow rates during high water that cause a dilution effect for the mercury concentration upstream and its accumulation downstream. The water quality varied from excellent to very poor with better quality during the high-water period. The Lom watershed is locally affected by physical and chemical pollution due to the abundance of suspended solids and mercury resulting from the different gold mining activities.

Keywords: artisanal gold mining; Lom river basin; upstream Sanaga basin; physical pollution; chemical pollution; water quality

Citation: Bella Atangana, M.S.; Ndam Ngoupayou, J.R.; Deliege, J.-F. Hydrogeochemistry and Mercury Contamination of Surface Water in the Lom Gold Basin (East Cameroon): Water Quality Index, Multivariate Statistical Analysis and Spatial Interpolation. *Water* **2023**, *15*, 2502. https://doi.org/10.3390/w15132502

Academic Editor: Luisa Bergamin

Received: 5 June 2023
Revised: 4 July 2023
Accepted: 5 July 2023
Published: 7 July 2023

1. Introduction

Surface water accounts for a small percentage (0.26%) of the world's freshwater and represents an essential natural resource for human life and activities [1]. It is therefore essential to preserve the good ecological status for sources of freshwater [2]. However, demographic growth and increasing needs emphasize the pressures on the water resource [1], making it more sensitive to pollutants from various natural and anthropogenic sources [2]. Among the pressures on surface water, artisanal and small-scale gold mining (AGSM) is of particular importance [3,4]. Small-scale gold mining has been practiced for centuries around the world. It is a source of economic development and livelihood for people in many developing countries in sub-Saharan Africa, Asia, South America and Oceania [5]. In the eastern Cameroon region, the Lom River and its tributaries drain the Lom gold-bearing catchment, where gold mining has been practiced in an artisanal manner since the 1950s [6] and been semi-mechanized since the boom of extractive industries in Africa in the 2000s. This period was characterized by the arrival of foreign mining companies (mainly Chinese) equipped with modern machinery [7]. Semi-mechanized mining is more efficient than artisanal mining because it uses machinery such as excavators, shovels, washing units and

dredges. This type of mining is mainly used for shallow deposits that are less than 20 m deep [8]. There are nearly one hundred semi-mechanized open-pit mines in the eastern region, which had a production of approximately 318 kg of gold in 2019 [9]. Gold mining is the source of many environmental, social and health problems, which include the use of mercury and environmental contamination [10]. Indeed, mercury emissions from gold mining represents nearly 38% of the total global emissions [11]. In this type of exploitation, mercury is often used to extract the gold ore from the gangue by amalgamation; the UNEP [12] estimates that it takes 1 to 2 g of mercury to process 1 g of gold. Mercury is used in the ore extraction process as it facilitates the recovery of fine gold particles. After extraction and crushing, the ore is treated by adding mercury to form an amalgam of equal proportions of Hg and gold, which is then heated (400–500 °C) to preserve the spongy gold and evaporate the Hg (Smith, 2019; Kosai et al., 2023). Mercury is thus released into the environment (atmosphere, soil, water) at different stages of processing; the World Gold Council [13] estimates that 5 to 45% of the mercury used is directly released in its elementary form into rivers.

Numerous worldwide works in mining areas report the degradation of the physicochemical quality of water resources due to this activity [14–23]. This degradation is especially due to the contamination by heavy metals and various pollutants, as well as the increase in the rate of erosion by the excavation work that enriches waters with sediment and particulate matter. In general, several approaches are currently used to assess water quality, including the calculation of quality indexes [24,25], numerical modeling [26,27], multivariate statistical analysis [22,28], etc. Most of the studies in the Lom Basin have focused on the structural geology and geochemistry of gold-enriched formations [29–34]. Few studies have focused on water quality or specifically on heavy metal pollution [22,35–37], showing that the basin's water quality is threatened by mining activity. However, no study on mercury contamination has been conducted in the Lom watershed. This is regretful, especially considering the project to supply drinking water from the Sanaga River [38] below the confluence with the Lom River. Indeed, the project involves the construction of catchment and pumping stations to produce 300.000 m^3/d to solve the drinking water deficit in Yaoundé and its surroundings. This work aims at (1) seasonal monitoring of classical physicochemical parameters to assess the water quality and identify the potential origins of pollution and (2) assessing the mercury contamination and the associated health risks for the riverside population using raw water. A combined approach of water quality index (WQI) calculation, multivariate statistical analysis (MSA) and spatial interpolation (IDW) was used.

2. Materials and Methods

2.1. Study Area

2.1.1. Geographical Setting

The Lom gold-bearing watershed (11100 km^2) is located in the East Region of Cameroon (Figure 1). The climate is a typical equatorial transition type, characterized by (i) a long dry season (from December to April), (ii) a transition period (from May to June) and (iii) a heavy rainy season from July to November [35]. The mean annual temperature is 24.7 °C, and the annual average rainfall is between 1500 and 2000 mm. The dominant vegetation found in the area is a dense semi-deciduous forest of medium altitude with an advanced stage of degradation due to mining [22]. The study area belongs to the geomorphological unit known as the South Cameroon Plateau, which has average altitudes that vary between 600 and 1100 m [39]. Its relief is rugged and dominated by gently sloping hills interspersed with swampy lowlands. The Lom Basin is drained by a dense hydrographic network, of which the Lom River is the main watercourse. With a length of about 370 km, the Lom is one of the main left-bank tributaries of the Sanaga River [40]. In recent years, the Lom River Basin has been affected by intense mining activity and the construction of the Lom–Pangar dam downstream of the watershed.

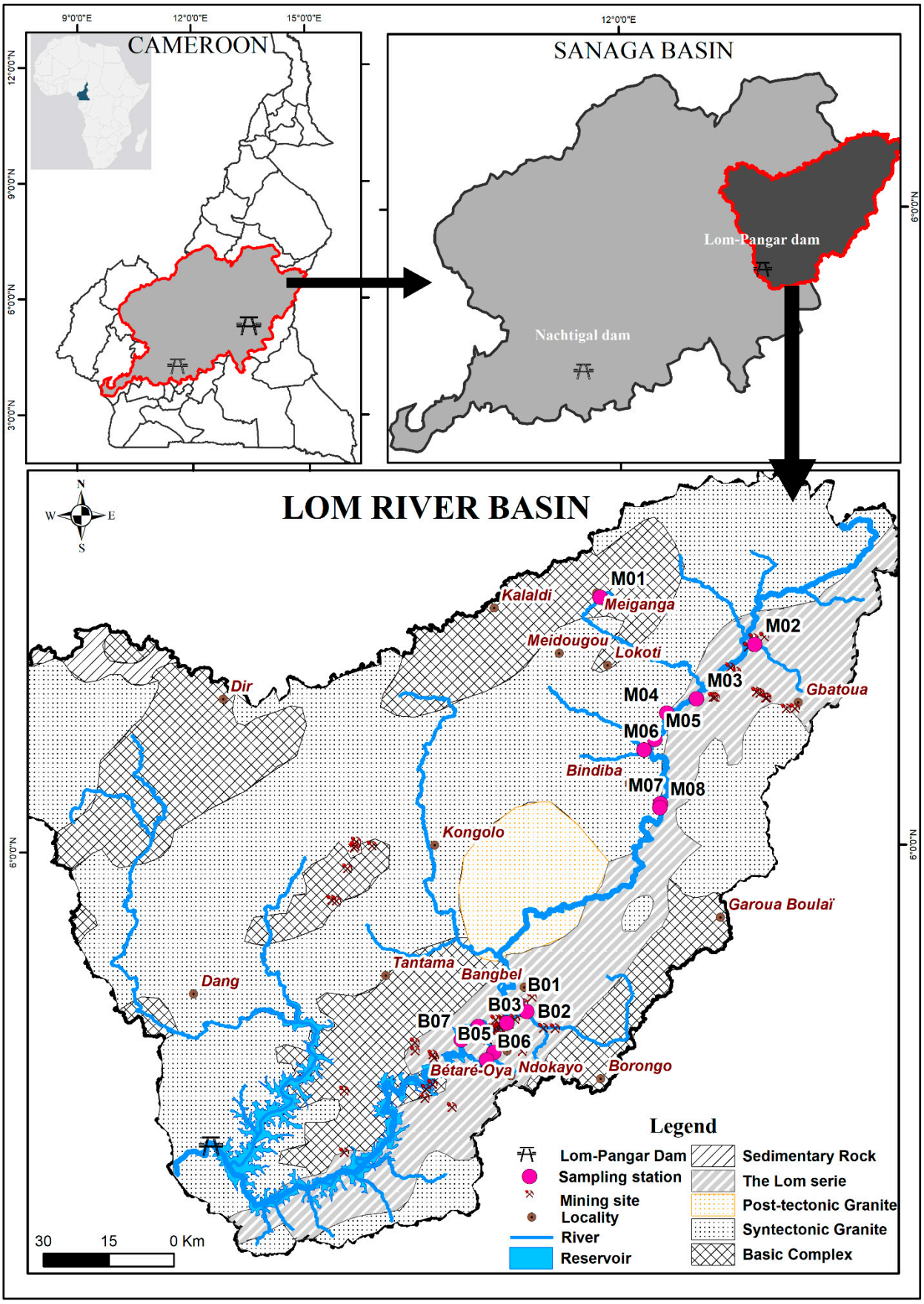

Figure 1. Location map of the Lom Basin, showing sampling stations and geological context.

2.1.2. Geological and Hydrogeological Setting

The Lom watershed belongs to the Cameroonian pan-African basement of the Precambrian age. The dominant geological formations in the area are metasedimentary and metavolcanic rocks [41]. They are composed of schists, mica schist, quartzites, orthogneiss and intrusive granites (of Wakasso and Ndokayo). These rocks are known as the "Lom series" and contain metamorphic–hydrothermal mineralization of a polymetallic nature [29,30,41,42]. Some of these rocks include sulfide-bearing quartz veins containing pyrite and gold [31,43], which are the origin of the intense artisanal mining in the area. Over these geological formations, the pedological cover consists mainly of thick red or brown ferralitic soils at high altitudes and darker hydromorphic soils in the swamps and alluvial plains [39,44]. Hydrogeologically, groundwater is abundant and is housed in two types of aquifers that are superposed or isolated depending on the case [45]: (a) the upper aquifer of overlying residual rocks that is continuous (<20 m) and (b) the deep fractured and/or fissured discontinuous aquifer (between 20 and 100 m).

2.2. Sampling and Analytical Procedure

Two field campaigns were carried out during the year 2021: the first one in March for sampling during the low-water period (40 m^3/s < flow < 106 m^3/s) and the second one in September for sampling during the high-water period (120 m^3/s < flow < 430 m^3/s), to represent the hydrological regime of the basin. Fifteen sampling stations were positioned in two sectors, one representative of the upstream part of the basin (Meiganga sector: M01 to M08) and the other of the downstream part (Bétaré-Oya sector: B01 to B07). The stations were ideally located in urban areas and mining villages, downstream of mining sites under exploitation and abandoned mining sites. Physical parameters: the potential of hydrogen (pH), temperature (T), electrical conductivity (EC), dissolved oxygen (DO) and total dissolved solids (TDS) were measured in situ using a previously calibrated multiparameter (SIERINO AZ86031). A total of 30 surface water samples were collected from the Lom River and its main tributaries. Teflon bottles (500 mL) were place about 30 to 50 cm under the surface of the water in to collect the samples; these were then stored at 4 °C according to Rodier's protocol [46].

In the laboratory, the samples were filtered using cellulose membrane filters (0.45 µm) that had been previously dried in the oven (at 105 °C) and divided into two groups.

The first group was conditioned (100 mL borosilicate brown glass bottles kept at 4 °C) and sent to the laboratory (The International Institute of Tropical Agriculture) for analysis of total mercury (Hg) by inductively coupled plasma emission spectroscopy (ICP-EOS) using an Optima 8000 apparatus. Samples were preserved with 15 mL HCl and 6 mL potassium bromide bromate reagent (Merck quality, Darmstadt, Germany and/or its affiliates) per 100 mL for at least 24 h before the analysis. All mercury compounds were converted to divalent mercury by oxidation with Kbr/$KBrO_3$ (Merck quality). The solution was then reduced to the elemental form using 0.3% NaBH4 (Merck quality) in 0.5% NaOH (Merck quality) solution. Water samples were digested with 0.5 mL 10% hydroxylamine hydrochloride solution (Merck quality) until the sample became colorless. Then, the volumetric flask was brought to volume (50 mL) with ultra-pure water. An amount of 1% ascorbic acid solution was added to the digested sample to eliminate free brome. The prepared samples were vaporized in an induced argon plasma to undergo atomization, ionization and thermal excitation for detection and quantification by the optical emission spectrometer.

The second group was used for analyzing major cations (sodium (Na^+), ammonium (NH_4^+), potassium (K^+), magnesium (Mg^{2+}), calcium (Ca^{2+}) and anions (bicarbonate (HCO_3^-), chloride (Cl^-), fluoride (F^-), nitrate (NO_3^-), phosphate (PO_4^{3-}) and sulfate (SO_4^{2-}) by chromatography on ICS 90 and ICS 1000 models, respectively. The amount of suspended solids (TSS) was determined by drying (105 °C) and weighing the filters before and after filtration.

2.3. Data Analysis

2.3.1. Hydrochemical Modeling

Piper's and Gibbs's diagrams were used to determine the hydrochemical type of the water samples and the hydrogeochemical processes that led to the ionic load of the studied waters, respectively. The multilanguage hydrochemistry software "DIAGRAMMES", developed by Roland SIMLER at the Hydrogeology lab of Avignon, was used to generate and visualize the ionic triangular typology of the water (http://www.lha.univ-avignon.fr/, accessed on 2 September 2022). Excel 2013 software was used to generate the modified Gibbs diagram, as well as the dispersion diagrams of the ions.

2.3.2. Multivariate Statistical Analysis

Pearson's correlation matrix (CM) was used to assess the relationship between the 17 measured variables [47]. Principal component analysis (PCA) was used to identify homogeneous groups of variables within the principal factors to determine their possible origins as sources of pollution in the analyzed waters [48]. Finally, hierarchical cluster analysis (HCA) was used to explore the similarities between different sampling stations to better differentiate the likely pollution sources based on their locations, sampling periods and/or types of activity [22]. All these analyses were performed with XLSTAT (2022) software (https://www.xlstat.com/fr, accessed on 2 September 2022).

2.3.3. Calculation of Water Quality Index (WQI)

In this study, the weighted arithmetic method was used to calculate the water quality index [36,48]. The parameters representing acidification (pH), particulate matter (TSS), organic and oxidizable matter (DO, NH_4^+, NO_3^- and PO_4^{3-}), mineral content (EC, TDS, Ca^{2+}, Mg^{2+}, Na^+, K^+, Cl^- and SO_4^{2-}) and toxicity (Hg) were selected. The water quality index (Equation (1)) is the sum of the sub-indexes (*SI*) of each parameter (Equation (2)). The quality rating scale (*qi*) for each parameter is calculated by Equation (3). A relative weight (***Wi***) ranging from 1 to 5 is assigned to each parameter according to its importance in assessing drinking water quality (Equation (4)). The highest weight is assigned to parameters that have critical effects on the quality of water intended for human consumption compared with the limits recommended by the World Health Organization (WHO) [49].

$$WQI = \sum_{i=1}^{n} SIi \quad (1)$$

$$SI = Wi \times qi \quad (2)$$

$$qi = \frac{Ci}{Si} \times 100 \quad (3)$$

$$Wi = \frac{wi}{\sum_{i=1}^{n} wi} \quad (4)$$

q_i indicates the quality score, C_i is the concentration of each chemical parameter and S_i is the WHO [50] guideline value; SI_i is the sub-index of the '*i*th' parameter, W_i is the relative weight of each parameter, *Wi* is the weight assigned to each parameter and *n* is the number of parameters. The calculated relative weight values (W_i) and corresponding quality ranges are given in Tables 1 and 2, respectively.

Table 1. Relative weights of parameters.

Parameters	Units	Standards WHO	Weight (*Wi*)	Relative Weight (W_i)
pH		8.5	4	0.093
EC	µS/cm	1400	4	0.093
DO	mg O_2/L	8	4	0.093
TDS	mg/L	500	2	0.046
TSS	mg/L	40	2	0.046
Na^+	mg/L	200	2	0.046
NH_4+	mg/L	0.5	2	0.046
K^+	mg/L	12	1	0.023
Mg^{2+}	mg/L	125	2	0.046
Ca^{2+}	mg/L	75	2	0.046
HCO_3^-	mg/L	130	3	0.069
F^-	mg/L	1.5	2	0.046
Cl^-	mg/L	250	3	0.069
NO_3^-	mg/L	50	4	0.093
SO_4^{2-}	mg/L	250	4	0.093
Hg tot	mg/l	0.001	5	0.116

Table 2. Water quality ranges.

WQI	Rating of Water Quality	Grading
<50	Excellent water quality	A
50–100	Good water quality	B
100–200	Poor water quality	C
200–300	Very poor water quality	D
>300	Unsuitable for drinking purposes	E

2.3.4. Calculation of Hazard Quotient (HQ) and Hazard Index (HI)

The hazard quotient (HQ) and hazard index (HI) from direct ingestion and dermal absorption in adults and children were calculated to assess the level of health risk to the riverside populations that are exposed to mercury toxicity in the Lom basin. Equations (5)–(9) were used following the method proposed by [51–53] based on risk guidelines of the US EPA [54], as shown in Table 3.

$$\text{ADDingestion} = \frac{Cw \times IR \times ABSg \times EF \times ED}{BW \times AT} \quad (5)$$

$$\text{ADDdermal} = \frac{Cw \times SA \times Kp \times EF \times ET \times ED \times 0.001}{BW \times AT} \quad (6)$$

$$\text{HQingestion} = \text{ADDingestion}/\text{RfDingestion} \quad (7)$$

$$\text{HQdermal} = \text{ADDdermal}/\text{RfDdermal} \quad (8)$$

$$\text{HI} = \sum(\text{HQingestion} + \text{HQdermal}) \quad (9)$$

where $ADD_{ingestion}$ and ADD_{dermal} are the average daily ingestion and dermal absorption dose in µg/kg/day, respectively; Cw is the mercury concentration (µg/L); *BW* is the average body weight (70 kg for adults and 15 kg for children); *IR* is the ingestion rate (2 and 0.64 L/day for adults and children); *EF* is the frequency of exposure (365 days/year); *ED* is the duration of exposure (years); *ABSg* is the gastrointestinal absorption factor (dimensionless); *SA* is the surface area of exposed skin (cm^2); *Kp* is the skin permeability

coefficient in water (cm/h); *ET* is the exposure time (h/day); *AT* is the averaging time (days) and *RfD* is the corresponding reference dose (µg/kg/day).

Table 3. Reference values for the parameters considered for mercury.

	Mercury (Hg)	Sources
ABSg	10%	[52,53,55]
Kp	0.001	[56]
RfDingestion	0.3	[52,53,55]
RfDdermal	0.086	[52,53,55]

For HQ > 1, non-carcinogenic effects should be considered; when HI > 1, carcinogenic effects on human health should be noted.

2.3.5. Geostatistical Modeling: Spatial Interpolation of Mercury Concentrations

The spatial distribution of mercury in the Lom basin was performed by interpolation between different measured concentrations at river points using an inverse distance weighting (IDW) method in the ArcGIS 10.8 software. The IDW spatial analysis tool considers that the influence of the plotted variable (mercury content) decreases with distance from the sampled location [57].

3. Results and Discussion

3.1. Physicochemical Characterization of Waters

3.1.1. Seasonal and Spatial Variation of Parameters

Physical Parameters

Table 4 shows the statistics for measured parameters at the sampling stations alongside the Lom River during the high-water and low-water periods. The charge balance error was less than ±10% for all the samples. The pH varies from 5.2 (min) to 6.6 (max) with an average of 5.90 during the low-water period and from 5.5 (min) to 7.1 (max) with an average of 6.43 during the high-water period. This represents slightly acidic to neutral waters. In general, the acidity of the basin increases from upstream to downstream for each period. However, the waters are more acidic during the low-water period, and the lowest measured pH values could be related to the oxidation of the sulfides contained in ores [31]. The nearly neutral pH values could be due to non-reactive sulfide minerals or due to rocks containing materials that neutralize the acidity [17]. These values are similar to those obtained for surface waters found in other mining environments [22,58,59]. The electrical conductivity (EC) oscillates between 12.80 (min) and 93.40 (max) with a mean of 39.94 µS/cm during the low-water period, whereas it varies from 16.10 (min) to 52 (max) with a mean of 31.74 µS/cm during the high-water period. The amounts of the various substances dissolved (TDS) in the water affects the water's conductivity, with higher levels of TDS leading to higher conductivity. During the low-water period, the TDS levels range from 9 (min) to 65 (max) mg/L, with an average of 28 mg/L, whereas during the high-water period, the range is from 11.24 (min) to 36.32 (max) mg/L and the average is 22.16 mg/L. According to Boeglin et al. [60], such (extremely low) dissolved concentrations indicate that the chemical weathering is very slow and this range for the TDS (<1000 mg/L) refers to fresh waters [61,62]. Physical parameters such as pH, EC and TDS are below the European Environmental Quality Standards [63] for drinking water limit values, as well as those of the WHO [50]. On the other hand, the total suspended solids (TSS) value exceeded the EQS and WHO guidelines (>25–40 mg/L) in some stations during the low-water period (LW: min = 12 mg/L, max = 452 mg/L, avg = 149 mg/L; HW: min = 2.62 mg/L, max = 20.90 mg/L, avg = 10.05 mg/L). High levels of suspended solids are generally found in mining areas where mining activities (deforestation, land excavation, riverbed dredging, ore panning and washing) increase particle erosion [3,22,64].

Major Ions

The abundances of major ions (Table 4), according to their average concentrations, during the low-water period is in the order $Na^+ > K^+ > SO_4^{2-} > Cl^- > Ca^{2+} > Mg^{2+} > NO_3^- > NH_4^+ > F^- > PO_4^{3-}$ vs. $Na^+ > Ca^{2+} > Mg^{2+} > SO_4^{2-} > Cl^- > K^+ > NO_3^- > NH_4^+ > F^- > PO_4^{3-}$ during the high-water period. The major ions are all below the limits of the WHO and EQS standards for each period. In general, the concentrations of dissolved substances are more abundant during the high-water period than during the low-water period. This reflects the transport mechanism in humid tropical areas where (i) the ionic load of swampy areas (where the rock mineral dissolution is intense) and (ii) the various inputs (atmospheric, vegetation and anthropogenic) are easily mobilized during the rainy season [36,60,65]. However, the major ions remain very low and reflect a large cation deficit as well as an anion deficit during the low-water period (TZ^+ max = 132.88 µeq/L and TZ^- max = 375.75 µeq/L) compared with other rivers in the world [66]. This is due to (i) the very thick ferralitic soils that protect the bedrock from chemical weathering [67] and (ii) the drained granitic bedrock that is mainly composed of more inert materials that do not significantly ionize the waters [68]. The predominance of cations (Ca^{2+}, Mg^{2+}, Na^+ and K^+) is typical of the weathering of the plutonic and metamorphic rocks that constitute the geologic basement due to the weathering of plagioclase and primary feldspars [67,69].

Table 4. Statistics on the measured parameters at sampling stations alongside the Lom River during the low-water and high-water periods.

Period			Low Water/Dry Season				High Water/Wet Season				Standards	
Parameters	**N**	**Units**	**Min**	**Max**	**Avg**	**SD**	**Min**	**Max**	**Avg**	**SD**	**WHO (2017)**	**EQS (2008)**
pH	15		5.23	6.59	5.90	0.56	5.57	7.08	6.43	0.53	6.5–8.5	6.5–8.5
T	15	°C	18.10	28.30	23.16	2.36	22.80	36.80	26.31	3.76	25	30
EC	15	µS/cm	12.80	93.40	39.94	19.98	16.10	52.00	31.74	9.16	1500	800
DO	15	mg/L	5.00	7.40	5.74	0.68	1.50	6.30	3.82	1.76	-	2–6
TDS	15	mg/L	9.00	65.00	28.00	13.90	11.24	36.32	22.16	6.40	500	
TSS	15	mg/L	12.00	452.00	149.00	152.01	2.62	20.90	10.05	5.47	25–40	25–40
Alka	15	µmol/L	41.89	373.21	182.08	78.51	0.57	51.63	15.13	15.24	-	-
Na^+	15	mg/L	0.052	0.991	0.394	0.330	1.444	6.104	3.501	1.476	200	200
NH_4^+	15	mg/L	0.001	0.328	0.048	0.084	0.047	0.846	0.329	0.258	0.5	3
K^+	15	mg/L	0.037	0.845	0.266	0.238	0.217	2.604	1.175	0.824	12	
Mg^{2+}	15	mg/L	0.014	0.453	0.132	0.115	5.248	36.976	17.492	9.349	125	
Ca^{2+}	15	mg/L	0.040	0.367	0.148	0.096	16.032	65.642	29.083	14.817	75	75
TZ^+	15	µeq/L	11.29	132.87	62.14	41.88	1899.41	5840.52	3112.46	1280.78	-	-
HCO_3^-	15	mg/L	2.55	22.8	11.120	4.791	0.57	51.64	15.13	15.24	130	-
F^-	15	mg/L	0.003	0.075	0.015	0.017	0.064	0.277	0.168	0.071	2	2
Cl^-	15	mg/L	0.014	0.669	0.195	0.190	0.348	2.240	1.185	0.510	250	250
NO^{3-}	15	mg/L	0.011	0.481	0.132	0.145	0.090	1.221	0.540	0.336	50	50
PO_4^{3-}	15	mg/L	0.000	0.002	0.000	0.001	0.000	0.067	0.013	0.021	1.5	5
SO_4^{2-}	15	mg/L	0.059	1.231	0.213	0.287	0.658	24.149	4.512	6.035	150	250
TZ^-	15	µeq/L	48.699	375.74	194.811	77.146	82.580	1034.187	392.191	286.745	-	-
Hg tot	15	mg/L	0.001	0.031	0.007	0.008	0.000	0.042	0.008	0.013	0.006	0.0007

Notes: Min = minimum, Max = maximum, Avg = average, SD = standard deviation, TZ^+ = sum of cations, TZ^- = sum of anions, WHO = Word Heath Organization, EQS = Environmental Quality Standard.

3.1.2. Water Hydrochemistry

Hydrochemical Classification

The projection of the water composition in the Piper diagram [70] led to a hydrochemical classification of the analyzed waters as well as their spatiotemporal evolution (Figure 2). During the low-water period and in the upstream part of the basin, the waters are of the bicarbonate–calcic and magnesian type at 62.5% against 37.5% for the bicarbonate–sodium and potassium types. Downstream of the watershed, the waters are divided into three types:

chloride–sulfate–calcic and magnesian at 42.86%, bicarbonate–sodic–potassic at 42.86% and bicarbonate–calcic–magnesian at 14.28%. During the high-water period, the hydrochemical classes of the waters evolved, changing to be 100% the calcic–bicarbonate type in the upstream sector. In the downstream sector, the waters changed from the three previous types to two types: bicarbonate–calcic–magnesian at 57.14% and bicarbonate–calcic at 42.86%.

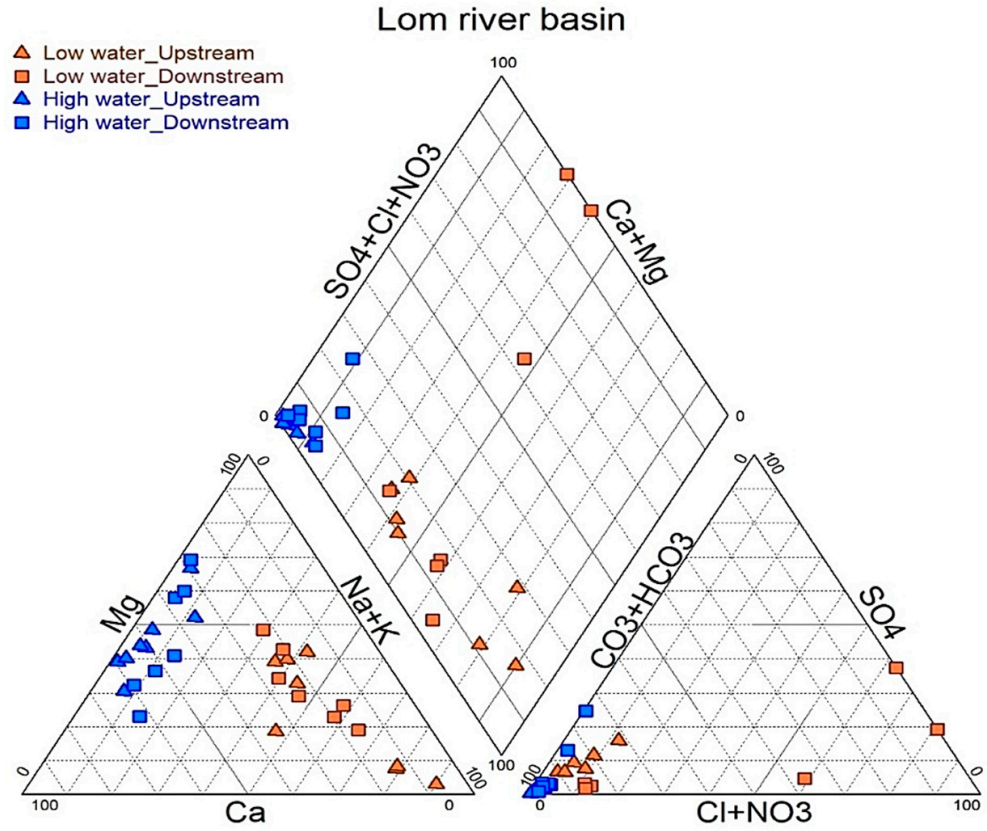

Figure 2. Piper diagram showing the hydrochemical facies of the waters.

In general, the predominant types in the analyzed waters are mainly bicarbonate–calcic (Ca-HCO_3) at 36.66% and bicarbonate–calcic–magnesian (CaMg-HCO_3) at 33.33%. These classes are typical of surface waters flowing over metamorphic rocks in tropical forests [71] and characterize the dissolution processes of primary silicate minerals [22,35].

Saturation Index

The saturation index (SI) is used to describe the thermodynamic equilibrium of the waters in terms of dissolved minerals (logarithm of the ratio between the ionic activity product Q and the mineral equilibrium constant K, SI: log (SI) = log (Q/K) = logQ − logK). Calculation of the saturation index in PHREEQC-2.7 software shows that Lom waters are undersaturated (SI < 0) in carbonate minerals (aragonite, calcite and dolomite), sulfate minerals (gypsum and anhydrite) and in CO_2, H_2O and O_2 whatever the season (Table 5). This corroborates the cationic and anionic deficits reported above and is in line with other results from the same basin [36].

3.1.3. Origins of the Parameters

Processes Controlling Water Chemistry

Gibbs [72] identifies atmospheric precipitations, rock weathering and evaporation–crystallization processes as the three main natural mechanisms controlling worldwide surface water chemistry. He set up a diagram depicting the weight ratio of

Na/(Na + Ca) versus cations and Cl/(Cl + HCO_3) versus TDS to determine the origins of dissolved geochemical constituents.

Table 5. Saturation index.

Season	Sector	Mineral Phase	Anhydrite	Aragonite	Calcite	Dolomite	Gypsum	H_2(g)	H_2O(g)	Halite	O_2(g)	CO_2(g)
Low water	Up stream	Min	−7.50	−7.38	−7.24	−14.60	−7.28	−21.18	−20.99	−13.19	−46.18	−3.55
		Max	−6.39	−5.28	−5.13	−9.87	−6.02	−6.16	−1.43	−1.59	−14.95	−2.16
		Mean	−6.99	−5.83	−5.68	−11.22	−6.74	−18.80	−3.98	−11.00	−39.03	−3.00
		Standard	0.37	0.75	0.75	1.58	0.41	5.18	6.87	3.85	9.89	0.43
	Down stream	Min	−7.39	−6.95	−6.80	−13.43	−28.31	−18.87	−19.21	−19.24	−47.27	−2.09
		Max	−6.54	−5.75	−5.61	−10.82	−6.31	−7.16	−1.52	−1.55	−11.82	−1.56
		Mean	−7.01	−6.17	−6.03	−11.80	−9.99	−15.59	−4.84	−11.13	−37.19	−1.75
		Standard	0.28	0.49	0.49	1.01	8.10	5.27	6.63	5.13	16.01	0.20
High water	Up stream	Min	−4.04	−1.47	−1.32	−2.59	−8.25	−22.05	−3.69	−22.18	−40.78	−1.88
		Max	−3.58	−0.22	−0.07	−0.15	−2.77	−2.38	−1.49	−9.85	−5.54	−1.34
		Mean	−3.79	−0.85	−0.71	−1.32	−5.55	−7.79	−3.02	−18.81	−14.39	−1.57
		Standard	0.16	0.38	0.38	0.78	1.90	7.17	0.77	4.39	12.41	0.20
	Down stream	Min	−4.19	−2.45	−2.31	−4.91	−12.55	−20.63	−3.27	−19.41	−44.23	−1.20
		Max	−2.74	−1.73	−1.59	−3.13	−2.51	−2.48	−1.22	−9.61	−5.88	−0.31
		Mean	−3.52	−2.16	−2.02	−3.89	−5.77	−15.06	−1.88	−12.62	−31.46	−0.79
		Standard	0.49	0.27	0.27	0.69	4.09	8.54	0.81	4.56	17.56	0.28

The sample results plotted in the Gibbs diagram (Figure 3) show that, in general, precipitation and rock weathering are the primary mechanisms that dominate in the Lom basin. Atmospheric precipitation controls most of the water chemistry during the high-water period, whereas rock weathering dominates during the low-water period. Similar to our observations, data related to the world's major rivers that drain tropical areas (Congo, Orinoco and Niger) were in the "precipitation control-rock control" series. Indeed, the chemical composition of low salinity waters is controlled by the rate of dissolved salts supplied by precipitation. This is precisely the case for tropical rivers in Africa and South America that have their source in low relief areas where the supply rate of dissolved salts to rivers is very low and the amount of precipitation is high [72]. These results are comparable with those of Rakotondrabe et al. [22] in the Lom basin, those of Mfonka et al. and Kamtchueng et al. [47,73] in the West Region of Cameroon and those of Thalmeier et al. [74] in Argentina, where rock weathering processes predominate the rainfall ones.

Different processes can occur during the rock–water interactions. The plot of total cations versus alkalinity (Figure 4a) indicates that mineral dissolution is the primary process controlling the chemistry of the studied waters. Furthermore, in the scatter plot of (Ca + Mg) versus (HCO_3 + SO_4), the majority (80%) of samples fall below the theoretical equilibrium line (Figure 4b). This result suggests that silicate weathering is the main source of ions [75], especially since the bedrock is composed of primary silicate minerals. Mimba et al. [35] suggest that silicate hydrolysis (plagioclases and feldspars) by the slightly acidic water of the basin is at the origin of the dissolved cations. The scattering of samples (negative and non-significant correlation) in Figure 4c eliminates the probability that nitrate derives from nitrification during the degradation of organic matter. In which case the generation of nitrate would consume the alkalinity [76]. Finally, the dispersion of Na as a function of Cl (Figure 4d) indicates that atmospheric inputs are not the only source of sodium in the analyzed waters and that sodium is also derived from cation exchange [73].

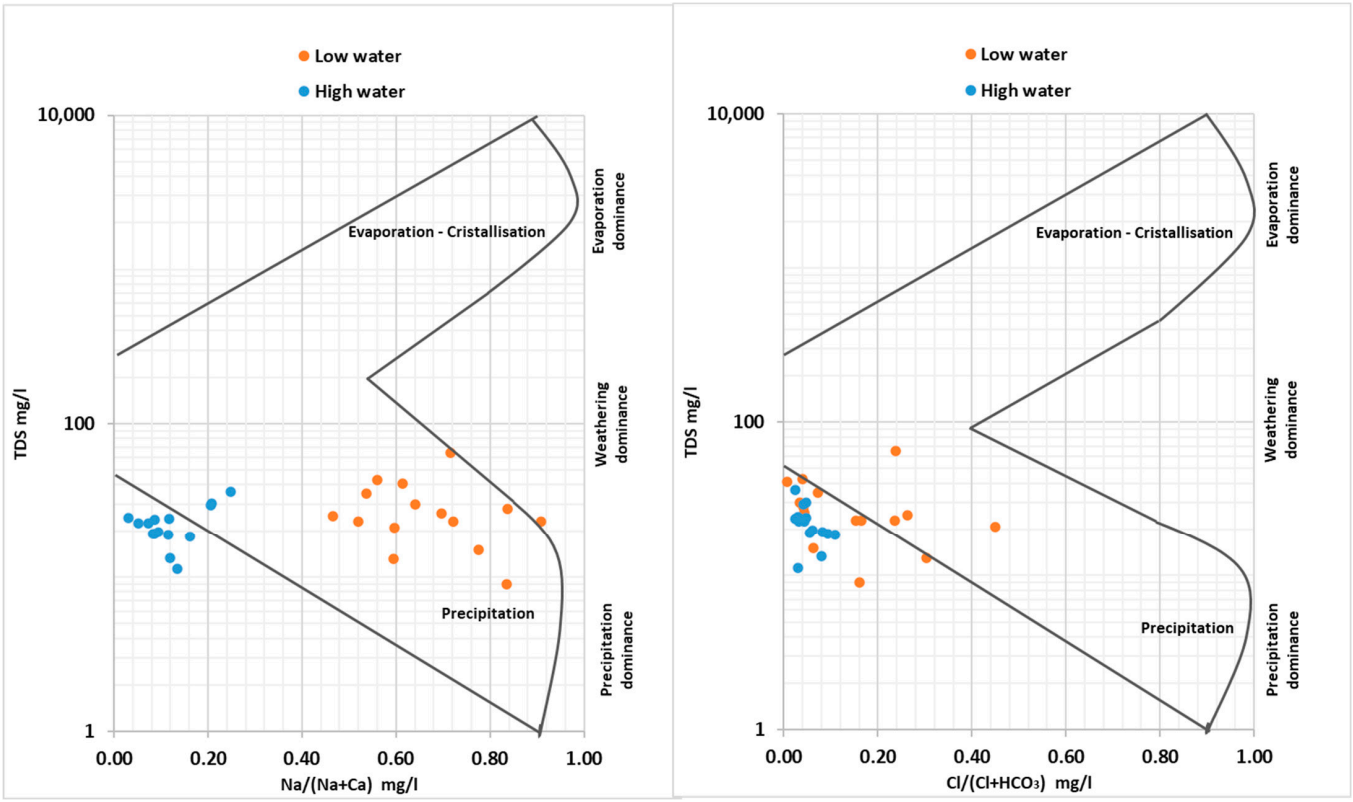

Figure 3. Gibbs diagrams showing the mechanisms controlling the water chemistry of Lom waters: (**left**) Variation of the weight cations ratio Na/(Na + Ca) as a function of total dissolved salts. (**right**) Variation of the weight anions ratio Cl/(Cl + HCO_3) as a function of total dissolved salts.

Correlation Tests

To properly identify the relationships between the variables for each season, two Pearson correlation matrices were produced, one for the low-water period (Figure 5a) and one for the high-water period (Figure 5b). The matrices show very strong ($0.7 < r < 1$), strong ($0.5 < r < 0.7$) and acceptable ($0.3 < r < 0.5$) positive (+) or negative (−) correlation coefficients between some variables (TDS–EC, K^+–Na^+, Ca^{2+}–Mg^{2+}, SO_4^{2-}–F^- and Hg–TSS).

During the low-water period, the Pearson correlation matrix shows (i) very strong positive correlations between TDS and EC, SO_4^{2-} and F^-, K^+ and Na^+, Ca^{2+} and Mg^{2+}, and b NO_3^-, Cl^- and F^-; (ii) strong positive correlations between DO and alkaline earth metals (Mg^{2+} and Ca^{2+}), NO_3^- and SO_4^{2-}, Ca^{2+} and Na^+, and Hg, TSS and EC; and finally, (iii) a strongly negative correlation was found between dissolved oxygen (DO) and dissolved solids and conductivity (TDS and EC). During the high-water period, the matrix shows (i) very strong positive correlations between TDS and EC, K^+ and TSS, and DO and pH; (ii) a strong positive correlation between Ca^{2+}, pH and DO; and (iii) an acceptable correlation between Hg and TSS.

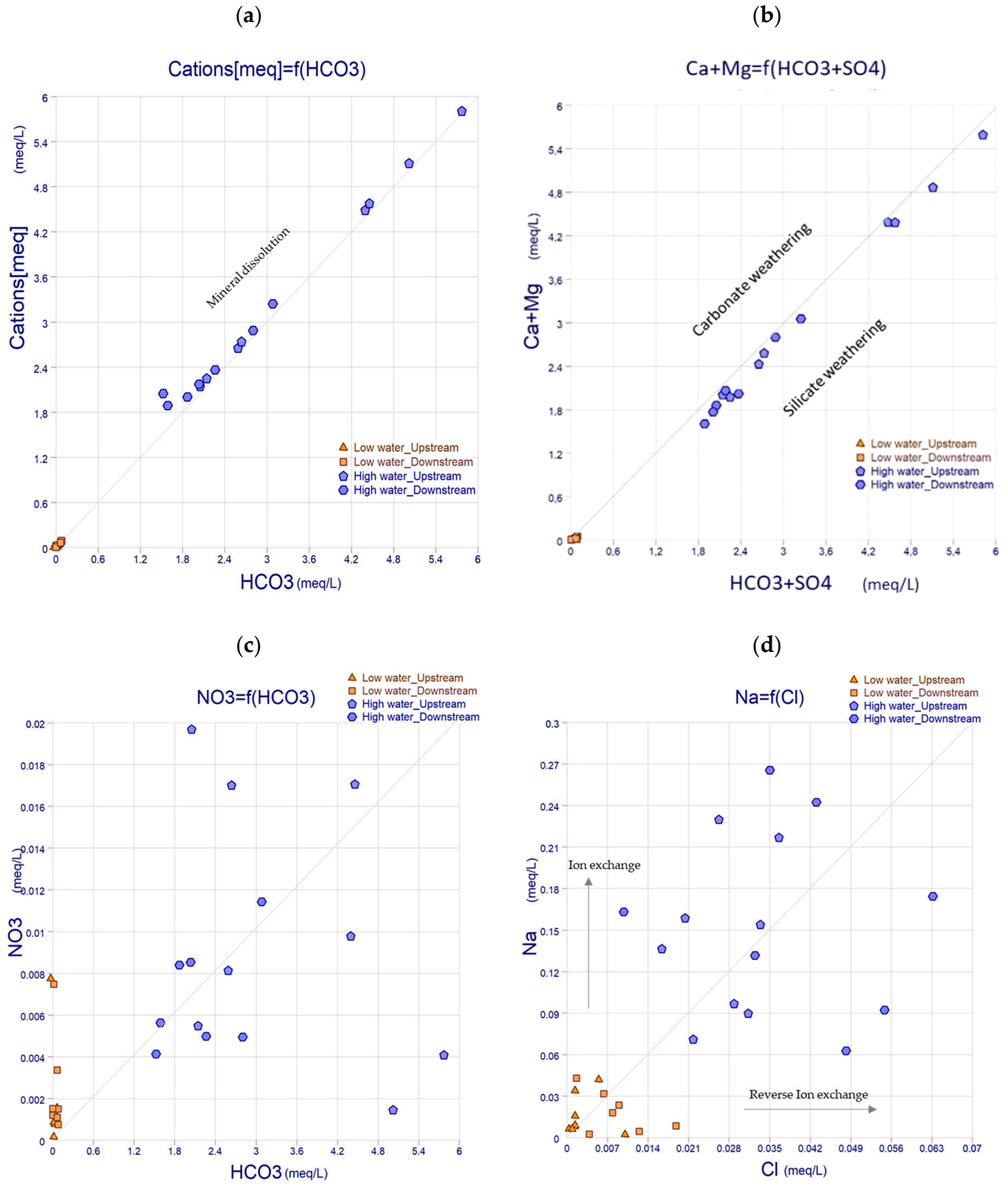

Figure 4. Mechanisms governing runoff chemistry: (**a**) mineral dissolution, (**b**) silicate weathering, (**c**) nitrification and (**d**) ion exchange for sodium.

The correlation matrix highlights the link between some variables and the geological nature of the drained terrains. Among these, the alteration of granites and metamorphic rocks whose dissolution of potassium feldspars (orthoses) and plagioclases would be the

origin of major cations (K^+ and Na^+, Ca^{2+} and Mg^{2+}) [36,69,77]. The alteration of schists, specifically the oxidation of sulfide ores (pyrite) contained in the gold-bearing veins to which fluorine is generally associated, is at the origin of SO_4^{2-} and F^- [78]. The strong correlation between TSS and Hg in the low-water period could reflect the importance of the mercury adsorption phenomenon on the surface of very fine TSS, which present larger specific surfaces. In the absence of published particle size analysis data from the Lom Basin, data from the Sanaga Basin (to which the Lom Basin belongs) were used. Indeed, the work of Ndam et al. [79] in the Sanaga Basin shows that suspended solids are mainly made up of very fine mineral fractions (90% silts and clays and 10% organic fraction) that can explain the adsorption phenomenon of Hg on TSS. During the high-water period, the weak link between Hg and TSS can be explained by the high flows that are capable of transporting larger particles that have smaller specific surfaces. The particle size analysis in the Sanaga River sediments shows that they are mostly composed (76 to 100%) of unworn quartz grains [79] that offer smaller specific surfaces. These observations corroborate those of the Amazon basin, where high Hg concentrations in white waters (Rio Madeira) are mainly due to the high loads of suspended material from intense erosion during the rainy season [80]. Moreover, the study by Guédron et al. [81] in the Lower Mekong River Basin shows that Hg is preferentially adsorbed to the specific surface of very fine suspended particles during its transport, in contrast to quartz sands, which have a low adsorption capacity.

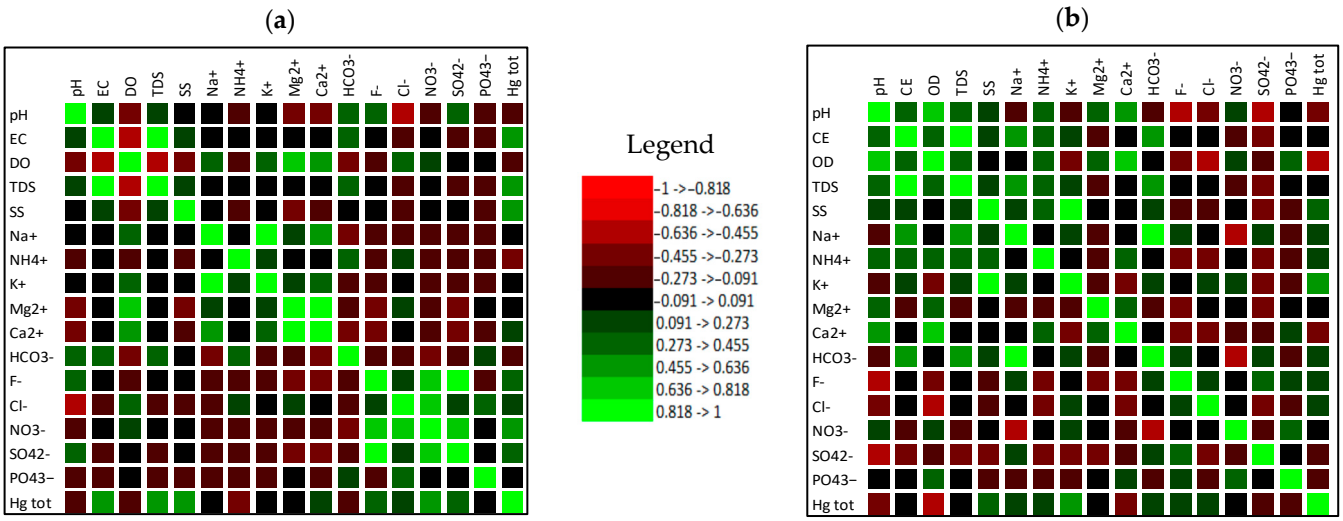

Figure 5. Correlation between physicochemical parameters: (**a**) low water and (**b**) high water.

Pollutants Sources: Principal Component Analysis (PCA)

PCA (Table 6) of the data collected during the two periods (dry season and rainy season) in the year 2021 produced 16 components or factors (F1–F16) representing the total variability of the dataset. According to the eigenvalue criterion, only factors with eigenvalues >1 were considered significant. Thus, factors F1 to F5, which represent 78.2% of the variability of the data, were used to identify the main types of pollution encountered in the analyzed waters. The correlations between variables and factors are considered very strong for $0.7 < r < 1$ and strong for $0.5 < r < 0.7$.

The F1 plane (38.57%) is very strongly to strongly composed of the variables NH_4^+, K^+, NO_3^-, Mg^{2+}, Ca^{2+}, Na^+, Cl^- and F^-. F1 represents the component of mineralization resulting from various hydrogeochemical processes, such as the dissolution of silicate minerals, ion exchange on clay minerals and soil leaching, or from anthropogenic activities, such as agriculture, livestock and domestic wastewater discharge [82,83]. F2 (13.70%) shows a very strong association with EC and TDS and a strong link with Hg. This component is associated with the dissolved solids load and toxicity that are likely from gold mining

activities, such as the discharge of mining effluents containing Hg and the erosion of mine tailings [22]. The component F3 (12.25%) is linked to the pH and DO variables that characterize the acid/alkaline nature of the water and the consumption of dissolved oxygen for the degradation of organic matter. F3 designates the organic pollution of the waters [84]. The F4 factor (7.44%) is strongly related to sulfates (SO_4^{2-}); it reflects the presence of shale or pollution by domestic wastewater [62]. Finally, F5 (6.57%) is composed of the characteristic variables of the contributions of agriculture activities (PO_4^{3-} and NO_3^-).

Table 6. Correlations between variables, principal factors and eigenvalues.

	F1	F2	F3	F4	F5
pH	0.420	0.114	0.707	−0.029	−0.157
EC	−0.358	0.833	0.254	0.290	−0.009
OD	−0.594	−0.296	0.596	−0.036	0.061
TDS	−0.362	0.830	0.254	0.290	−0.009
TSS	−0.629	0.268	−0.082	−0.035	0.182
Na^+	0.818	0.170	−0.058	0.231	−0.286
NH_4^+	0.597	0.182	0.350	−0.240	−0.224
K^+	0.663	0.302	−0.221	−0.351	−0.052
Mg^{2+}	0.797	0.000	0.259	−0.096	−0.049
Ca^{2+}	0.800	−0.048	0.431	0.094	−0.101
F^-	0.866	0.084	−0.231	0.275	0.130
Cl^-	0.819	0.120	−0.212	−0.152	0.008
NO_3^-	0.671	0.048	0.143	−0.199	0.514
PO_4^{3-}	0.424	−0.111	0.271	0.302	0.715
SO_4^{2-}	0.436	−0.183	−0.403	0.658	−0.119
Hg tot	0.091	0.642	−0.432	−0.323	0.191
Eigenvalues	6.17	2.19	1.96	1.19	1.05
Variability (%)	38.57	13.70	12.25	7.44	6.57
Cumulative %	38.57	52.27	64.53	71.97	78.54

The analysis of the correlation circle (Figure 6) following the F1/F2 axes, regrouping 52.28% of the variance and presenting the highest eigenvalues (6.17 and 2.19, respectively), was used to identify the main types of pollution in the Lom water. Two groups stand out:

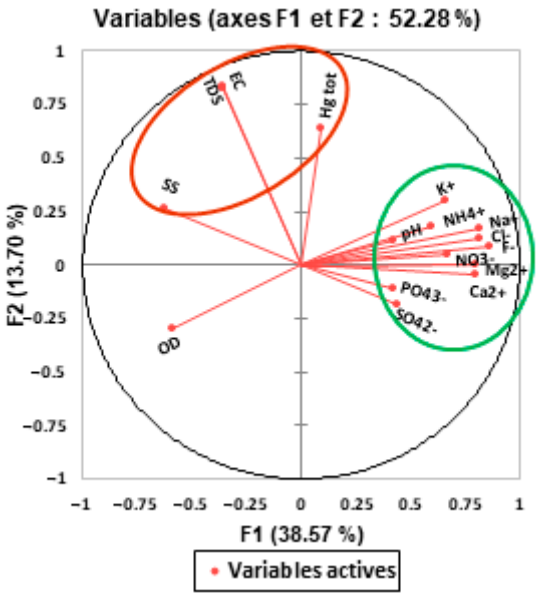

Figure 6. Correlation circle of variables following the F1/F2 axes.

Group 1—green circle, which includes the major ions (Na^+, K^+, Mg^{2+}, Ca^{2+}, NH_4^+, NO_3^-, SO_4^{2-}, Cl^-, F^- and PO_4^{3-}) and pH. This group is characteristic of mineralization from natural origins (mainly from the dissolution of silicate minerals, soil leaching, atmospheric inputs and/or vegetation) or anthropogenic activities (agriculture, livestock and domestic wastewater). The variables of Group 1 are all below the recommended limits from the WHO and EQS.

Group 2—red circle, consists of EC, TDS, TSS and Hg. The first three variables represent the dissolved matter load (mineral and organic) and Hg constitutes the toxicity due to mercury introduced during ore processing by amalgamation and discharged in the mining effluents. Suspended solids (TSS) represent the particulate load from land excavation and tailing erosion and gold-panning activities.

Both TSS and Hg locally exceeded the recommended limits for drinking water (WHO and EQS) and the Cameroonian discharge standard (CDS). These two variables indicate that the two main types of pollution affecting the study waters are chemical pollution due to mercury toxicity and physical pollution due to suspended solids. Indeed, Rakotondrabe et al. [22] and Achina-Obeng and Aram [4] also found high concentrations of TSS, heavy metals and mercury in the Mari catchment (eastern Cameroon) and the Central Region of Ghana that were mainly due to gold mining activities (digging of rivers beds, excavation and gold amalgamation).

3.2. Mercury Contamination of Water

3.2.1. Water Quality Index (WQI)

The calculation of the water quality index (WQI) from the physicochemical parameters (pH, EC, TDS, TSS, HCO_3^-, Cl^-, SO_4^{2-}, Na^+, Ca^{2+}, Mg^{2+}, NO_3^-, F^- and Hg) was used to evaluate the water quality of the Lom Basin. The Lom's water quality varies from excellent to very poor (Figure 7).

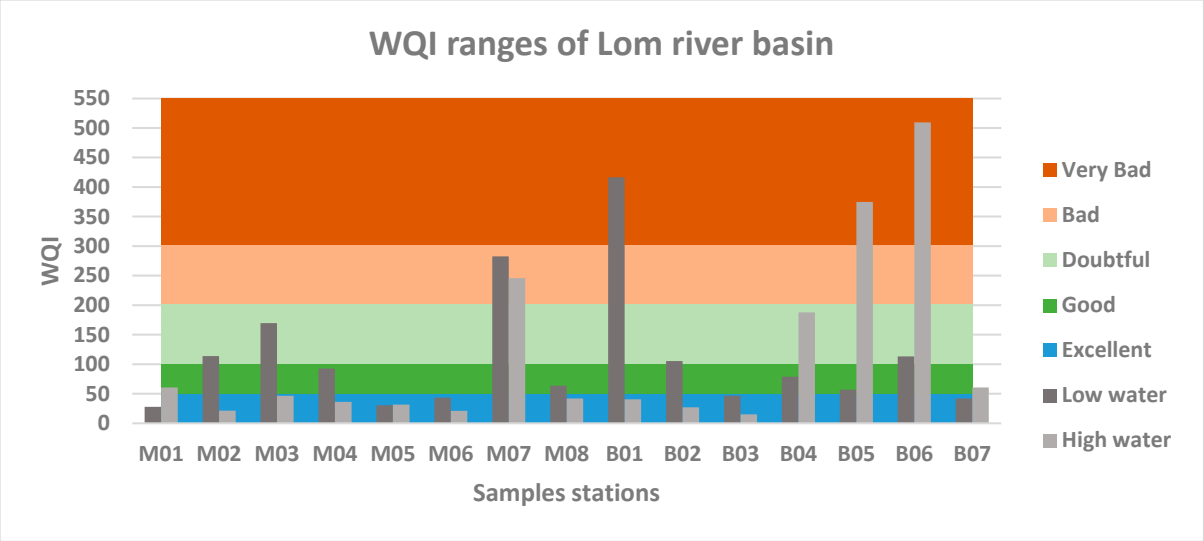

Figure 7. Water quality ranges in the Lom River Basin by season.

During the low-water period, nearly 60% of the waters are of excellent to good quality (WQI < 100), compared with 40% of the waters that were doubtful to very poor quality (WQI > 100). During the high-water period, a greater proportion of samples have excellent to good quality (73%) and only 26.69% have very poor quality. Globally, water quality is better during the high-water season. The water quality degrades from upstream to downstream of the basin, and the highest WQI values (WQI > 100) are found on the mainstream (M03, M07, B04 and B06), whereas the tributaries are of better quality (WQI < 100). This is probably due to the dilution of the water by the abundant precipita-

tion during this season. These results are quite similar to the observations of [36] in the same basin.

3.2.2. Spatial and Seasonal Distribution of Mercury

Hierarchical Cluster Analysis (HCA)

To distinguish the sampling periods, samples collected during the low-water period will be assigned the letter D at the beginning of the corresponding station code (DM01, . . . , DB07) and those collected during the high-water period will be assigned the letter W (WM01, . . . , WB01). The dendrogram obtained by HCA (Figure 8) clusters the different sampling stations into two main classes (C1 and C2).

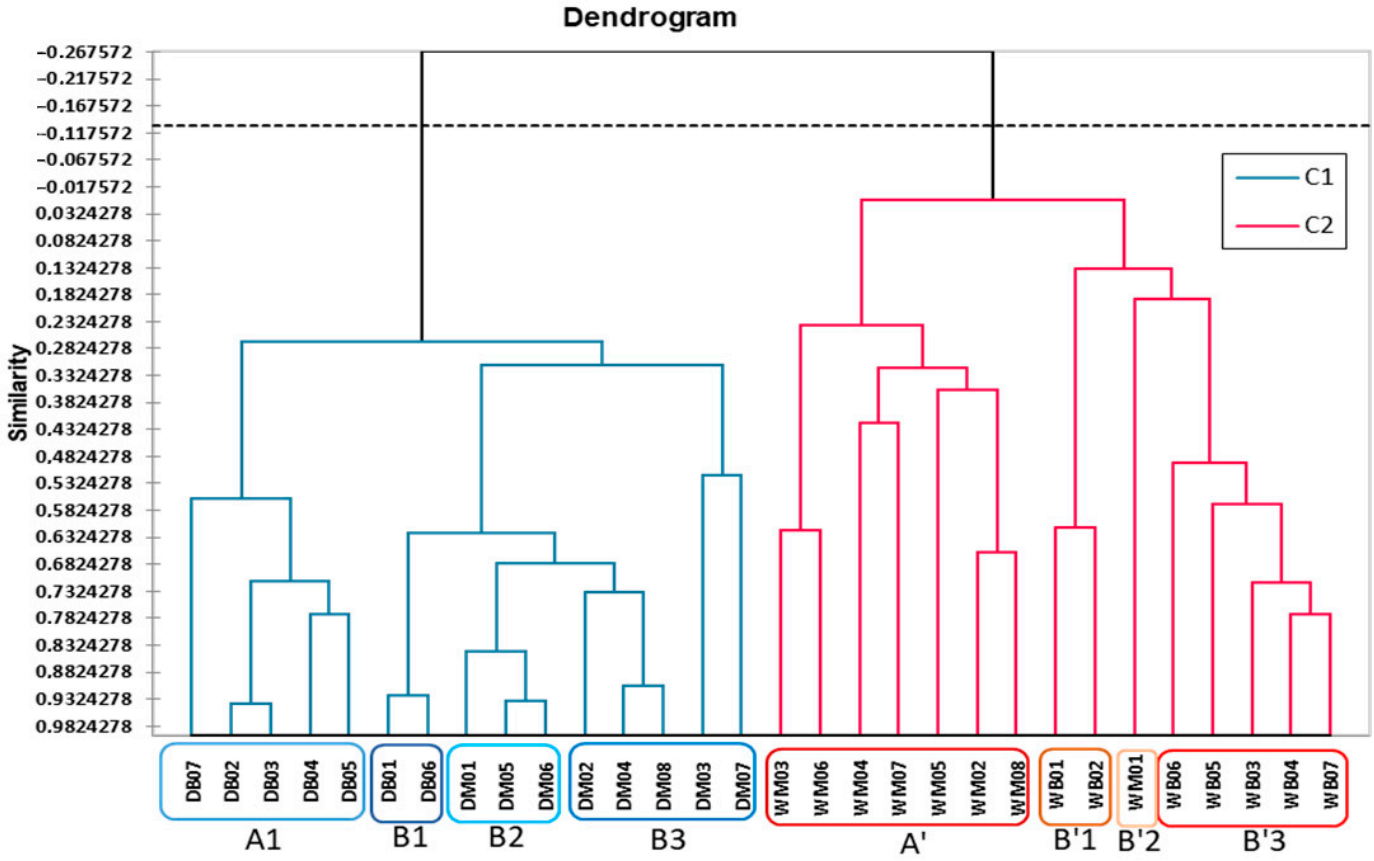

Figure 8. Dendrogram showing the spatiotemporal groupings of the sampling stations.

Class C1 includes all samples taken during the low-water period (dry season) and can be subdivided into two subclasses (A and B). Subclass A is composed of station DB07 (in an urban area) and stations DB02 to DB05, which are all located in the Bétaré-Oya sector, downstream of the watershed. The latter stations are mainly located in mining villages that are downstream of mining sites that are mostly in reduced activity due to the low flows of the season. Subclass A represents sites with acceptable mercury levels in the downstream part of the basin ($2 < Hg < 5$ µg/L). Subclass B can be subdivided into three groups (B1, B2 and B3). Group B1 stations (DB01 and DB06) are located downstream of intense exploitation areas and have Hg concentrations that are moderate to very high (8 µg/L and 31 µg/L). Group B1 represents moderately and heavily polluted sites downstream of the basin. Group B2 is formed of stations DM01, DM05 and DM06, which are located in urban areas upstream of the watershed where mercury levels are acceptable ($1 < Hg < 2$ µg/L). This group contains unpolluted sites from the upstream part of the basin. Group B3 includes stations DM02, DM04, DM08, DM03 and DM07, which are located in the intense exploitation areas in the upstream basin. The mercury levels range from

4 to 21 µg/L and the activity is mainly on the Lom River. Group B3 represents the moderately to heavily polluted sites in the upstream part of the basin.

Class C2 is entirely composed of samples collected during the high-water period (wet season). It can also be separated into two sub-classes (A′ and B′). Subclass A′ includes stations located upstream of the basin, either downstream of the mining sites (WM02 to WM08) or in an urban area (WM06). The mercury concentrations for this group are acceptable (0 < Hg < 2 µg/L), except for station WM07 (Hg = 19 µg/L), where mining was carried out using a dredge in the riverbed. Subclass B′ can be divided into three groups (B′1, B′2 and B′3). The first group (B′1) is composed of stations WB01 and WB02 that are located in the downstream sector of the basin, in a washing pool and downstream of an operating site. The mercury levels are acceptable (2 µg/L and 1 µg/L, respectively); these stations are unpolluted sites downstream of the basin. Group B′2 is composed of station WM01, which is located in the urban area of the basin's upstream sector and where the mercury content is also acceptable (Hg = 3 µg/L). Finally, Group B′3 is made up of stations WB03 to WB07, which are located in both mining villages and urban areas (WB07) in the downstream sector. These sites are highly polluted (15 < Hg < 42 µg/L), except for the urban area (Hg = 4 µg/L).

Sample stations have been clustered according to the sampling period (high-water–low-water), geographical location (upstream–downstream of the watershed) and the station's position relative to mining activities (upstream–downstream of mining sites). In general, for both periods, mercury levels are acceptable in urban areas when mining areas are moderately to heavily polluted. This reflects the localized mercury pollution near gold mining sites. These observations are similar to those from the Puyango River Basin in southwestern Ecuador [15]. In this study, mercury levels were very high in both seasons and showed a downstream concentration gradient with the highest Hg levels (250 ng Hg/L) adjacent to mining areas.

Spatial Interpolation of Mercury Concentrations

During the low-water period, the total mercury levels ranged from low (0.7 < Hgtot < 6 µg/L) to moderate (6.1 < Hgtot < 10 µg/L) and the quality (related to Hg) was better downstream than upstream in the basin. Hg remained below the Cameroonian discharge standard (CDS = 10 µg/L) for both sectors but exceeded WHO limits for drinking water upstream of the basin (<6 µg/L). During the high-water period, mercury concentrations changed from low to moderate (1 < Hgtot < 10 µg/L) upstream and reached high levels downstream (11 < Hgtot < 50 µg/L). The concentration of mercury decreases from the upstream to downstream part of the basin. The lowest Hg levels are found near mining areas upstream of the catchment, and Hg levels increase significantly downstream where the pollutant concentrates and exceeds the limits of all of the standards (>11 µg/L).

Mercury concentrations in the basin are very variable for many reasons. Firstly, the hydrological regime has a major influence on the variation of mercury levels in the basin. Indeed, heavy precipitation during the high-water season contributes to (i) the dilution of Hg upstream, (ii) the remobilization of sedimented fractions and (iii) the accumulation of the pollutant in the lower elevation floodplains downstream of the basin. This is due to the fact that in tropical regions, most of the transport of materials takes place during the high-water periods when heavy rainfall leaches the slopes, erodes the banks and remobilizes sediments from the bed [85]. Indeed, the same dynamic has been observed in Kazakhstani rivers, where mercury transport during spring floods is dominated by the remobilization of contaminated bed sediments and bank erosion [86]. The work of Carmouze et al. [80] on the Rio Madeira shows that the maximum concentrations of Hg were not recorded in the tributaries that were exploited for alluvial gold but 200 km downstream in the Andean foothills. This corroborates part of our results on the spatial variations of mercury concentrations near mining sites during the high-water period. These authors also found that Hg levels are higher during low-water periods than during high-water periods in the Amazon. This finding is the same for the Lom basin, except for stations located near

the floodplain downstream of the basin, where mercury concentrations are higher during floods. This could be due to increased mining activity during the high-water period or the presence of unrecorded mines in the area.

The results of the spatial interpolation by the inverse distance weighting method for the sampled sub-basins allowed the mapping of mercury contamination levels in the basin (Figure 9). The areas in dark green (0 < Hgtot < 0.7 µg/L) and light green (0.7 < Hgtot < 1 µg/L) have very low Hg levels that are below the European standards (EQS = 0.7 µg/L and WFD = 1 µg/L). The areas in yellow (1 < Hgtot < 6 µg/L) have acceptable Hg levels, but they are above the WHO standards (6 µg/L). The orange areas (6.1 < Hgtot < 10 µg/L) correspond to moderate pollution levels that are below the Cameroonian standards for industrial discharge (CSD = 10 µg/L). Finally, the red areas show high Hg pollution levels (Hgtot > 11 µg/L) exceeding all the above limits.

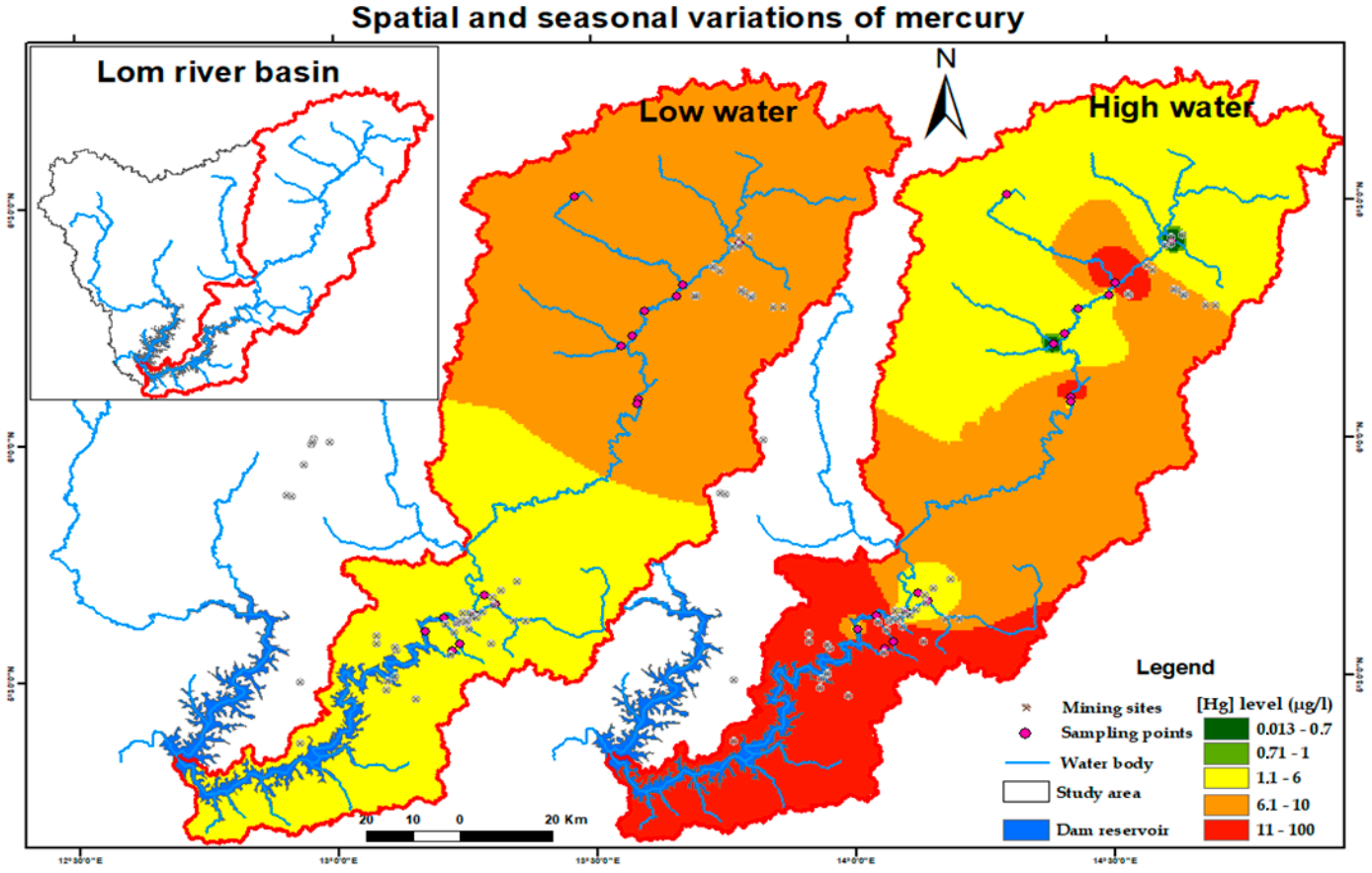

Figure 9. Spatial and seasonal variation of mercury concentrations in the Lom basin.

3.2.3. Human Health Risk for Mercury

The calculated values (µg/kg/day) of the hazard quotient (HQ) and the hazard index (HI) in the analyzed waters are shown in Table 7. The maximum daily ingestion dose is nearly two times higher for children ($HQ_{ingestion}$ Max = 0.573) and more than one time higher for adults ($HQ_{ingestion}$ Max = 0.383) than the reference value ($RfD_{ingestion}$ = 0.3). The dermal absorption dose is below the reference value for adults but twice the reference limit for children (RfD_{dermal} = 0.21). However, for both children and adults, the average daily ingestion doses, dermal absorption doses and the mercury hazard index are less than 1 ($HQ_{ingestion}$ < 1; HQ_{dermal} > 1 and HI < 1) regardless of season. This indicates that the mercury concentrations in the analyzed waters represent little danger for both children and adults in the riverside populations.

Table 7. Hazard quotient (HQingestion/dermal) and hazard index (HI) of mercury during the low- and high-water periods in the Lom Basin.

	HQingestion		HQdermal		HI (∑HQ)	
	Children	**Adults**	**Children**	**Adults**	**Children**	**Adults**
Total (∑)	3.080	2.060	1.110	3.76×10^{-1}	4.190	2.440
Min	0.000	0.000	0.000	0.000	0.000	0.000
Max	5.73×10^{-1}	3.84×10^{-1}	2.06×10^{-1}	6.98×10^{-2}	7.79×10^{-1}	4.53×10^{-1}
Average	1.03×10^{-2}	6.88×10^{-2}	3.70×10^{-2}	1.25×10^{-2}	0.140	8.13×10^{-2}
SD	1.46×10^{-1}	9.80×10^{-2}	5.26×10^{-2}	1.78×10^{-2}	1.99×10^{-1}	1.16×10^{-1}
RfDingestion	0.300	0.300	-	-	-	-
RfDdermal	-	-	0.086	0.086	-	-

Notes: Min = minimum, Max = maximum, SD = standard deviation.

As was observed in previous studies on soil and surface water samples in China and Spain [52,55,87,88], the $HQ_{ingestion}$ values are higher than the HQ_{dermal} values ($HQ_{ingestion} > HQ_{dermal}$). Oral ingestion was found to be the primary form of exposure to mercury for residents. Similarly, children have higher HQ and HI values (ingestion and dermal) than adults, indicating that children's health is more vulnerable to the adverse effects of mercury contamination. However, these results are only indicative because, for a better assessment of the health risk, methyl mercury (CH_3Hg) should have been analyzed, as it is the most toxic form of the pollutant found in living organisms.

4. Conclusions

This study shows that the physicochemical parameter concentrations of the Lom surface water are below the recommended WHO and European Standards for drinking water, except locally for suspended solids and total mercury. These waters have low mineral composition at the origin of the ionic deficit observed during the low-water period. The predominance of Ca^{2+}, Mg^{2+} and HCO_3^- ions converts waters the bicarbonate–calcic and bicarbonate–calcic and magnesian types. The spatial and seasonal variations in parameters highlight the typical hydrodynamics of tropical forest zones, where the ionic load is higher during the high-water period due to the mobilization of dissolved elements, as well as various inputs (atmospheric, vegetation and anthropic) during the heavy rainfall season. This also reflects that the water chemistry is mainly controlled by precipitation and silicate dissolution. The water physicochemical quality is better during the high-water period than during the low-water period and deteriorates from upstream to downstream. This is related to the dilution effect on the total Hg concentration upstream and its accumulation downstream. Except for direct mercury users, Hg represents little danger for both the children and adults of the riverside populations. However, (i) oral ingestion was found to be the main way of exposure for residents and (ii) children's health is more vulnerable to the adverse effects of mercury contamination. The Lom waters are affected by physical pollution (TSS) and chemical pollution (Hg) that are accentuated by and resulting from different gold mining activities. These two types of pollution confirm the key role of gold mining in the water quality degradation of the basin.

In general, this study constitutes a first approach and contributes to analyzing the Lom Basin according to the levels of mercury in surface water and the health risks incurred for the riverside populations. It completes the weak existing geochemical database. This is essential for the sustainable management of this hydrosystem, which is subjected to (i) intense artisanal and semi-mechanized gold mining and (ii) considering the PAEPYS project of supplying drinking water from the Sanaga River from below the confluence with the Lom River.

Author Contributions: Investigation, M.S.B.A. Conceptualization, J.R.N.N., J.-F.D. and M.S.B.A.; formal analysis, M.S.B.A.; Methodology, J.R.N.N., J.-F.D. and M.S.B.A.; Writing—original draft preparation, M.S.B.A.; Writing—Reviewing and Editing, M.S.B.A. and J.-F.D.; Visualization, J.-F.D., J.R.N.N. and M.S.B.A.; Validation, J.-F.D. and J.R.N.N.; Supervision, J.-F.D. and J.R.N.N.; Writing-Reviewing and Editing, J.-F.D. and M.S.B.A. All authors have read and agreed to the published version of the manuscript.

Funding: This research did not receive any specific grant from funding agencies in the public, commercial, or not-for-profit sectors.

Institutional Review Board Statement: Not applicable.

Informed Consent Statement: All authors have read and agreed to the final version of the manuscript.

Data Availability Statement: Data are available upon request from the corresponding author.

Acknowledgments: We thank the PeGIRE/AQUAPOLE laboratory, Faculty of Science, University of Liege, where this work was conducted. We also thank the Hydrogeology Laboratory of the Department of Earth Sciences, University of Yaoundé I, for documentary and fieldwork support. We also thank the Laboratory of Geochemical Analysis of Water (LAGE) of the Institute of Mining et geological Research (IRGM) of Yaoundé, as well as the laboratory of the International Institute of Tropical Agriculture (IITA) where the samples were analyzed.

Conflicts of Interest: The authors declare that they have no known competing financial interest or personal relationships that could have appeared to influence the work reported in this paper.

References

1. Abbott, B.W.; Bishop, K.; Zarnetske, J.P.; Hannah, D.M.; Frei, R.J.; Minaudo, C.; Chapin, F.S.; Krause, S.; Conner, L.; Ellison, D.; et al. A Water Cycle for the Anthropocene. *Hydrol. Process.* **2019**, *33*, 3046–3052. [CrossRef]
2. Parween, S.; Siddique, N.A.; Mahammad Diganta, M.T.; Olbert, A.I.; Uddin, M.G. Assessment of Urban River Water Quality Using Modified NSF Water Quality Index Model at Siliguri City, West Bengal, India. *Environ. Sustain. Indic.* **2022**, *16*, 100202. [CrossRef]
3. Gallo Corredor, J.A.; Humberto Pérez, E.; Figueroa, R.; Figueroa Casas, A. Water Quality of Streams Associated with Artisanal Gold Mining; Suárez, Department of Cauca, Colombia. *Heliyon* **2021**, *7*, e07047. [CrossRef]
4. Achina-Obeng, R.; Aram, S.A. Informal Artisanal and Small-Scale Gold Mining (ASGM) in Ghana: Assessing Environmental Impacts, Reasons for Engagement, and Mitigation Strategies. *Resour. Policy* **2022**, *78*, 102907. [CrossRef]
5. Quarm, J.A.; Anning, A.K.; Fei-Baffoe, B.; Siaw, V.F.; Amuah, E.E.Y. Perception of the Environmental, Socio-Economic and Health Impacts of Artisanal Gold Mining in the Amansie West District, Ghana. *Environ. Chall.* **2022**, *9*, 100653. [CrossRef]
6. Tchindjang, M.; Philippes, M.; Unusa, H.; Eric, V.; Igor, N.; Saha, F. Mines Contre Forêts et Conservation Au Cameroun: Enjeux de l'évaluation Environnementale Du Secteur Minier Pour Le Développement Durable Au Cameroun. In Proceedings of the Actes du Colloque du SIFEE, Antananarivo, Madagascar, 9 January 2017.
7. Weng, L.; Boedhihartono, A.K.; Dirks, P.H.G.M.; Dixon, J.; Lubis, M.I.; Sayer, J.A. Mineral Industries, Growth Corridors and Agricultural Development in Africa. *Glob. Food Secur.* **2013**, *2*, 195–202. [CrossRef]
8. Word Gold Council. *Leçons Tirées de la Gestion de l'interface Entre les Exploitations Minières Aurifères à Grande Échelle et Celles Artisanales et à Petite Échelle*; Word Gold Council: London, UK, 2022; p. 100.
9. MINMIDT. *Initiative Pour La Transparence Dans Les Industries Extractives au Cameroun*; MINMIDT: Yaoundé, Cameroon, 2019; p. 343.
10. Quispe Aquino, R.; Malone, A.; Smith, N.M.; García Zúñiga, F.F. Perceptions and Realities of Mercury Contamination in a Peruvian Artisanal and Small-Scale Gold Mining (ASGM) Community. *Environ. Res.* **2022**, *214*, 114092. [CrossRef] [PubMed]
11. UNEP Global Mercury Assessment 2018. Available online: http://www.unep.org/resources/publication/global-mercury-assessment-2018 (accessed on 2 February 2023).
12. UNEP National Action Plans (NAPs) for Artisanal and Small Scale Gold Mining (ASGM) Democratic Republic of the Congo (RDC) | Global Mercury Partnership. Available online: https://www.unep.org/globalmercurypartnership/what-we-do/artisanal-and-small-scale-gold-mining-asgm/national-action-plans (accessed on 2 February 2023).
13. World Gold Council. *Small-Scale and Artisanal Gold Mining*; Word Gold Council: London, UK, 2022.
14. Hilson, G. The Environmental Impact of Small-scale Gold Mining in Ghana: Identifying Problems and Possible Solutions. *Geogr. J.* **2002**, *168*, 57–72. [CrossRef]
15. Betancourt, O.; Narváez, A.; Roulet, M. Small-Scale Gold Mining in the Puyango River Basin, Southern Ecuador: A Study of Environmental Impacts AndHuman Exposures. *EcoHealth* **2005**, *2*, 323–332. [CrossRef]
16. Zwane, N.; Love, D.; Hoko, Z.; Shoko, D. Managing the Impact of Gold Panning Activities within the Context of Integrated Water Resources Management Planning in the Lower Manyame Sub-Catchment, Zambezi Basin, Zimbabwe. *Phys. Chem. Earth Parts ABC* **2006**, *31*, 848–856. [CrossRef]

17. Gomes, M.E.P.; Antunes, I.M.H.R.; Silva, P.B.; Neiva, A.M.R.; Pacheco, F.A.L. Geochemistry of Waters Associated with the Old Mine Workings at Fonte Santa (NE of Portugal). *J. Geochem. Explor.* **2010**, *105*, 153–165. [CrossRef]
18. Ingram, V.; Tieguhong, J.C.; Schure, J.; Nkamgnia, E.; Tadjuidje, M.H. Where Artisanal Mines and Forest Meet: Socio-Economic and Environmental Impacts in the Congo Basin: Where Artisanal Mines and Forest Meet. In *Natural Resources Forum*; Blackwell Publishing Ltd.: Oxford, UK, 2011; Volume 35, pp. 304–320. [CrossRef]
19. Bakia, M. East Cameroon's Artisanal and Small-Scale Mining Bonanza: How Long Will It Last? *Futures* **2014**, *62*, 40–50. [CrossRef]
20. Guédron, S.; Point, D.; Acha, D.; Bouchet, S.; Baya, P.A.; Tessier, E.; Monperrus, M.; Molina, C.I.; Groleau, A.; Chauvaud, L.; et al. Mercury Contamination Level and Speciation Inventory in Lakes Titicaca & Uru-Uru (Bolivia): Current Status and Future Trends. *Environ. Pollut.* **2017**, *231*, 262–270. [CrossRef]
21. Strady, E.; Dinh, Q.T.; Némery, J.; Nguyen, T.N.; Guédron, S.; Nguyen, N.S.; Denis, H.; Nguyen, P.D. Spatial Variation and Risk Assessment of Trace Metals in Water and Sediment of the Mekong Delta. *Chemosphere* **2017**, *179*, 367–378. [CrossRef] [PubMed]
22. Rakotondrabe, F.; Ndam Ngoupayou, J.R.; Mfonka, Z.; Rasolomanana, E.H.; Nyangono Abolo, A.J.; Ako Ako, A. Water Quality Assessment in the Bétaré-Oya Gold Mining Area (East-Cameroon): Multivariate Statistical Analysis Approach. *Sci. Total Environ.* **2018**, *610–611*, 831–844. [CrossRef]
23. Barenblitt, A.; Payton, A.; Lagomasino, D.; Fatoyinbo, L.; Asare, K.; Aidoo, K.; Pigott, H.; Som, C.K.; Smeets, L.; Seidu, O.; et al. The Large Footprint of Small-Scale Artisanal Gold Mining in Ghana. *Sci. Total Environ.* **2021**, *781*, 146644. [CrossRef]
24. Liou, S.-M.; Lo, S.-L.; Wang, S.-H. A Generalized Water Quality Index for Taiwan. *Environ. Monit. Assess.* **2004**, *96*, 35–52. [CrossRef]
25. Uddin, M.G.; Nash, S.; Rahman, A.; Olbert, A.I. A Comprehensive Method for Improvement of Water Quality Index (WQI) Models for Coastal Water Quality Assessment. *Water Res.* **2022**, *219*, 118532. [CrossRef]
26. Deliège, J.-F.; Everbecq, E.; Magermans, P.; Grard, A.; Bourouag, M.; Blockx, C. PEGASE, an Integrated River/Basin Model Dedicated to Surface Water Quality Assessment: Application to Cocaine. *Acta Clin. Belg.* **2010**, *65*, 42–48. [CrossRef]
27. Stehr, A.; Debels, P.; Romero, F.; Alcayaga, H. Hydrological Modelling with SWAT under Conditions of Limited Data Availability: Evaluation of Results from a Chilean Case Study. *Hydrol. Sci. J.* **2008**, *53*, 588–601. [CrossRef]
28. Tripathi, M.; Singal, S.K. Allocation of Weights Using Factor Analysis for Development of a Novel Water Quality Index. *Ecotoxicol. Environ. Saf.* **2019**, *183*, 109510. [CrossRef] [PubMed]
29. Ngako, V.; Affaton, P.; Nnange, J.M.; Njanko, T. Pan-African Tectonic Evolution in Central and Southern Cameroon: Transpression and Transtension during Sinistral Shear Movements. *J. Afr. Earth Sci.* **2003**, *36*, 207–214. [CrossRef]
30. Toteu, S.F.; Van Schmus, W.R.; Penaye, J.; Michard, A. New U–Pb and Sm–Nd Data from North-Central Cameroon and Its Bearing on the Pre-Pan African History of Central Africa. *Precambr. Res.* **2001**, *108*, 45–73. [CrossRef]
31. Suh, C.E. Sulphide Microchemistry and Hydrothermal Fluid Evolution in Quartz Veins, Batouri Gold District (Southeast Cameroon). *J. Cameroon Acad. Sci.* **2008**, *8*, 12.
32. Vishiti, A.; Suh, C.E.; Lehmann, B.; Shemang, E.M.; Ngome, N.L.J.; Nshanji, N.J.; Chinjo, F.E.; Mongwe, O.Y.; Egbe, A.J.; Petersen, S. Mineral Chemistry, Bulk Rock Geochemistry, and S-Isotope Signature of Lode-Gold Mineralization in the Bétaré Oya Gold District, South-East Cameroon. *Geol. J.* **2018**, *53*, 2579–2596. [CrossRef]
33. Azeuda Ndonfack, K.I.; Xie, Y.; Goldfarb, R.; Zhong, R.; Qu, Y. Genesis and Mineralization Style of Gold Occurrences of the Lower Lom Belt, Bétaré Oya District, Eastern Cameroon. *Ore Geol. Rev.* **2021**, *139*, 104586. [CrossRef]
34. Fon, A.N.; Suh, C.E.; Vishiti, A.; Ngatcha, R.B.; Ngang, T.C.; Shemang, E.M.; Egbe, J.A.; Lehmann, B. Gold Dispersion in Tropical Weathering Profiles at the Belikombone Gold Anomaly (Bétaré Oya Gold District), East Cameroon. *Geochemistry* **2021**, *81*, 125770. [CrossRef]
35. Mimba, M.E.; Ohba, T.; Nguemhe Fils, S.C.; Wirmvem, M.J.; Tibang, E.E.B.; Nforba, M.T.; Togwa Aka, F. Regional Hydrogeochemical Mapping for Environmental Studies in the Mineralized Lom Basin, East Cameroon: A Pre-Industrial Mining Survey. *Hydrology* **2017**, *5*, 15. [CrossRef]
36. Rakotondrabe, F.; Ngoupayou, J.R.N.; Mfonka, Z.; Rasolomanana, E.H.; Nyangono Abolo, A.J.; Asone, B.L.; Ako Ako, A.; Rakotondrabe, M.H. Assessment of Surface Water Quality of Bétaré-Oya Gold Mining Area (East-Cameroon). *J. Water Resour. Prot.* **2017**, *9*, 960–984. [CrossRef]
37. Ngounouno, M.A.; Ngueyep, L.L.M.; Kingni, S.T.; Nforsoh, S.N.; Ngounouno, I. Evaluation of the Impact of Gold Mining Activities on the Waters and Sediments of Lom River, Wakaso, Cameroon and the Restorative Effect of Moringa Oleifera Seeds. *Appl. Water Sci.* **2021**, *11*, 113. [CrossRef]
38. Molemba, M.; Djomo, N.; Landry, B. Implications Socioéconomiques Du Projet PAEPYS Dans La Mise En Valeur Des Territoires à La Périphérie Est de Yaoundé. *Revue Territoires Sud.* **2021**, *1*, 35–44. Available online: www.https://territoiressud.org (accessed on 4 July 2023).
39. Olivry, J.-C. *Fleuves et Rivières du Cameroun*; Monographie hydrologiques. MESRES/ORSTOM, 1986; 733p; ISBN 978-2-7099-0804-7. Available online: http://www.hydrosciences.fr/sierem/Bibliotheque/biblio/Cameroun.pdf (accessed on 4 July 2023).
40. Dubreuil, P.; Guiscafre, J.; Nouvelot, J.-F.; Olivry, J.-C. *Le Bassin de la Rivière Sanaga*; Monographies Hydrologiques ORSTOM; Office de la Recherche Scientifique et Technique Outre-Mer: Paris, France, 1975; ISBN 978-2-7099-0361-5.
41. Kankeu, B.; Greiling, R.O.; Nzenti, J.P. Pan-African Strike–Slip Tectonics in Eastern Cameroon—Magnetic Fabrics (AMS) and Structure in the Lom Basin and Its Gneissic Basement. *Precambr. Res.* **2009**, *174*, 258–272. [CrossRef]

42. Fouotsa, S.A.N.; Rigobert, T.; Negue Emmanuel, N.; Dawaï, D.; Joseph, P.; Tchunte Periclex Martial, F. Polyphase Deformation in the Mbé—Sassa-Bersi Area: Implications on the Tectono-Magmatic History of the Area and the Tectonic Evolution of the Tcholliré-Banyo and Central Cameroon Shear Zones (Central North Cameroon). *J. Geosci. Geomat.* **2018**, *6*, 41–54. [CrossRef]
43. Vishiti, A.; Etame, J.; Suh, C.E. Features of Gold-Bearing Quartz Veins in an Artisanal Mining-Dominated Terrain, Batouri Gold District, Eastern Region of Cameroon. *Episodes* **2019**, *42*, 199–212. [CrossRef]
44. Segalen, P. *Les Sols et la Géomorphologie du Cameroun*; Office de la Recherche Scientifique et Technique Outre-Mer: Paris, France, 1962; Volume 46.
45. Lachassagne, P.; Dewandel, B.; Wyns, R. The Conceptual Model of Hard Rock Aquifers and Its Practical Applications. In Proceedings of the Vingtièmes journées techniques du Comité FranCais d'Hydrogéologie de l'Association Internationale des Hydrogéo-logues, La Roche-sur-Yon, France, 11–13 June 2015.
46. Rodier, J.; Merlet, N.; Legube, B. *L'analyse de l'eau*, 9th ed.; Entièrement Mise à Jour; Dunod: France, Paris, 2009; ISBN 978-2-10-054179-9.
47. Mfonka, Z.; Kpoumié, A.; Ngouh, A.N.; Mouncherou, O.F.; Nsangou, D.; Rakotondrabe, F.; Takounjou, A.F.; Zammouri, M.; Ngoupayou, J.R.N.; Ndjigui, P.-D. Water Quality Assessment in the Bamoun Plateau, Western-Cameroon: Hydrogeochemical Modelling and Multivariate Statistical Analysis Approach. *J. Water Resour. Prot.* **2021**, *13*, 112–138. [CrossRef]
48. Chakravarty, T.; Gupta, S. Assessment of Water Quality of a Hilly River of South Assam, North East India Using Water Quality Index and Multivariate Statistical Analysis. *Environ. Chall.* **2021**, *5*, 100392. [CrossRef]
49. World Health Organization. *Guidelines for Drinking-Water Quality: Fourth Edition Incorporating*; World Health Organization: Geneva, Switzerland, 2017; ISBN 978-92-4-154995-0.
50. Cotruvo, J.A. 2017 WHO Guidelines for Drinking Water Quality: First Addendum to the Fourth Edition. *J. Am. Water Works Assoc.* **2017**, *109*, 44–51. [CrossRef]
51. Meng, Q.; Zhang, J.; Zhang, Z.; Wu, T. Geochemistry of Dissolved Trace Elements and Heavy Metals in the Dan River Drainage (China): Distribution, Sources, and Water Quality Assessment. *Environ. Sci. Pollut. Res.* **2016**, *23*, 8091–8103. [CrossRef] [PubMed]
52. Tian, Y.; Wen, Z.; Cheng, M.; Xu, M. Evaluating the Water Quality Characteristics and Tracing the Pollutant Sources in the Yellow River Basin, China. *Sci. Total Environ.* **2022**, *846*, 157389. [CrossRef] [PubMed]
53. Wang, M.; Gui, H.; Hu, R.; Zhao, H.; Li, J.; Yu, H.; Fang, H. Hydrogeochemical Characteristics and Water Quality Evaluation of Carboniferous Taiyuan Formation Limestone Water in Sulin Mining Area in Northern Anhui, China. *Int. J. Environ. Res. Public Health* **2019**, *16*, 2512. [CrossRef]
54. U.S. Environmental Protection Agency. *U.S. E.P.A's 2006 Clean Water Act Recognition Awards: Availability of Application and Nomination Information*; Notices—Federal Register; U.S. Environmental Protection Agency: Washington, DC, USA, 2006; Volume 71, pp. 23855–24550.
55. Zeng, X.; Wang, Z.; Wang, J.; Guo, J.; Chen, X.; Zhuang, J. Health Risk Assessment of Heavy Metals via Dietary Intake of Wheat Grown in Tianjin Sewage Irrigation Area. *Ecotoxicology* **2015**, *24*, 2115–2124. [CrossRef]
56. U.S. EPA (Environmental Protection Agency). 2006 Edition of the Drinking Water Standards and Health Advisories. 2006. EPA 822-R-06-013 Office of Water U.S. Environmental Protection Agency Washington, DC, USA, 2006. Available online: http://www.epa.gov/waterscience (accessed on 4 July 2023).
57. Watson, D.F.; Philip, G.M. A Refinement of Inverse Distance Weighted Interpolation. *Geo-Processing* **1985**, *2*, 315–327.
58. Kumar, S.; Islam, A.R.M.T.; Hasanuzzaman, M.; Salam, R.; Khan, R.; Islam, M.S. Preliminary Assessment of Heavy Metals in Surface Water and Sediment in Nakuvadra-Rakiraki River, Fiji Using Indexical and Chemometric Approaches. *J. Environ. Manag.* **2021**, *298*, 113517. [CrossRef]
59. Ewusi, A.; Sunkari, E.D.; Seidu, J.; Coffie-Anum, E. Hydrogeochemical Characteristics, Sources and Human Health Risk Assessment of Heavy Metal Dispersion in the Mine Pit Water–Surface Water–Groundwater System in the Largest Manganese Mine in Ghana. *Environ. Technol. Innov.* **2022**, *26*, 102312. [CrossRef]
60. Boeglin, J.-L.; Ndam, J.-R.; Braun, J.-J. Composition of the Different Reservoir Waters in a Tropical Humid Area: Example of the Nsimi Catchment (Southern Cameroon). *J. Afr. Earth Sci.* **2003**, *37*, 103–110. [CrossRef]
61. Freeze, R.A.; Cherry, J.A. *Groundwater*; Prentice-Hall: Englewood Cliffs, NJ, USA, 1979; ISBN 978-0-13-365312-0.
62. Wanda, E.M.M.; Chavula, G.; Tembo, F.M. Hydrogeochemical Characterization of Water Quality Evolution within Livingstonia Coalfield Mining Areas in Rumphi District, Northern Malawi. *Phys. Chem. Earth Parts ABC* **2021**, *123*, 103045. [CrossRef]
63. European Parliament. EQS Directive 2013/39/EU of the European Parliament and of the Council of 12 August 2013 Amending Directives 2000/60/EC and 2008/105/EC as Regards Priority Substances in the Field of Water PolicyText with EEA Relevance. *Off. J. Eur. Union* **2013**, *L226*, 1–17.
64. Ayiwouo, M.N.; Mambou Ngueyep, L.L.; Mache, J.R.; Takougang Kingni, S.; Ngounouno, I. Waters of the Djouzami Gold Mining Site (Adamawa, Cameroon): Physicochemical Characterization and Treatment Test by Bana Smectite (West, Cameroon). *Case Stud. Chem. Environ. Eng.* **2020**, *2*, 100016. [CrossRef]
65. Viers, J.; Dupre, B.; Braun, J.-J.; Deberdt, S.; Angeletti, B.; Ngoupayou, J.N.; Michard, A. Major and Trace Element Abundances, and Strontium Isotopes in the Nyong Basin Rivers Cameroon: Constraints on Chemical Weathering Processes and Elements Transport Mechanisms in Humid Tropical Environments. *Chem. Geol.* **2000**, *169*, 211–241. [CrossRef]
66. Martin, J.-M.; Meybeck, M. Transports dissous et particulaire de quelques éléments chimiques par les rivières en milieu tempéré. *Sci. Géol. Bull. Mém.* **1979**, *53*, 45–48.

67. Braun, J.-J.; Dupré, B.; Viers, J.; Ngoupayou, J.R.N.; Bedimo, J.-P.B.; Sigha-Nkamdjou, L.; Freydier, R.; Robain, H.; Nyeck, B.; Bodin, J.; et al. Biogeohydrodynamic in the Forested Humid Tropical Environment: The Case Study of the Nsimi Small Experimental Watershed (South Cameroon). *Bull. Soc. Géol. Fr.* **2002**, *173*, 347–357. [CrossRef]
68. Bhateria, R.; Jain, D. Water Quality Assessment of Lake Water: A Review. *Sustain. Water Resour. Manag.* **2016**, *2*, 161–173. [CrossRef]
69. Meybeck, M.; Meybeck, M. Global Chemical Weathering of Surficial Rocks Estimated from River Dissolved Loads. *Am. J. Sci.* **1987**, *287*, 401–428. [CrossRef]
70. Piper, A.M. A Graphic Procedure in the Geochemical Interpretation of Water-Analyses. *Trans. Am. Geophys. Union* **1944**, *25*, 914. [CrossRef]
71. Meybeck, M. *River Water Quality Global Ranges, Time and Space Variabilities, Proposal for Some Redefinitions*; SIL Proceedings 1922–2010; Taylor & Francis: Milton Park, UK, 1996; Volume 26, pp. 81–96. [CrossRef]
72. Gibbs, R.J. Mechanisms Controlling World Water Chemistry. *Sci. New Ser.* **1970**, *170*, 1088–1090. [CrossRef]
73. Kamtchueng, B.T.; Fantong, W.Y.; Wirmvem, M.J.; Tiodjio, R.E.; Takounjou, A.F.; Ndam Ngoupayou, J.R.; Kusakabe, M.; Zhang, J.; Ohba, T.; Tanyileke, G.; et al. Hydrogeochemistry and Quality of Surface Water and Groundwater in the Vicinity of Lake Monoun, West Cameroon: Approach from Multivariate Statistical Analysis and Stable Isotopic Characterization. *Environ. Monit. Assess.* **2016**, *188*, 524. [CrossRef]
74. Thalmeier, M.B.; Rodriguez, L.; Heredia, J.; Veizaga, E. Hydrogeological and Hydrochemical Framework of the Distal Section of the Salado-Juramento Fluvial Megafan (Bajos Submeridionales) in South America. *Sci. Total Environ.* **2022**, *824*, 153543. [CrossRef]
75. Edjah, A.K.M.; Akiti, T.T.; Osae, S.; Adotey, D.; Glover, E.T. Hydrogeochemistry and Isotope Hydrology of Surface Water and Groundwater Systems in the Ellembelle District, Ghana, West Africa. *Appl. Water Sci.* **2017**, *7*, 609–623. [CrossRef]
76. Kim, K.; Koo, M.-H.; Moon, S.-H.; Yum, B.-W.; Lee, K.-S. Hydrochemistry of Groundwaters in a Spa Area of Korea: An Implication for Water Quality Degradation by Intensive Pumping. *Hydrol. Process.* **2005**, *19*, 493–505. [CrossRef]
77. Braun, J.-J.; Marechal, J.-C.; Riotte, J.; Boeglin, J.-L.; Bedimo Bedimo, J.-P.; Ndam Ngoupayou, J.R.; Nyeck, B.; Robain, H.; Sekhar, M.; Audry, S.; et al. Elemental Weathering Fluxes and Saprolite Production Rate in a Central African Lateritic Terrain (Nsimi, South Cameroon). *Geochim. Cosmochim. Acta* **2012**, *99*, 243–270. [CrossRef]
78. Aragão, F.; Velásquez, L.N.M.; Galvão, P.; Vieira, L.C. Natural Hydrogeochemical Background Levels in the Carste Lagoa Santa Protection Unit, Minas Gerais, Brazil. *J. S. Am. Earth Sci.* **2021**, *105*, 102985. [CrossRef]
79. Ndam Ngoupayou, J.R.; Kpoumie, A.; Boeglin, J.-L.; Lienou, G.; Nfocgo, A.K.; Ekodeck, G.E. Transports solides et érosion mécanique dans un écosystème tropical d'Afrique: Exemple du bassin versant de la Sanaga au Sud—Cameroun. In Proceedings of the JSIRAUF (1res Journées Scientifiques Inter-Réseaux de l'AUF), Hanoi, Vietnam, 6–9 November 2007; p. 6.
80. Carmouze, J.-P.; Lucotte, M.; Boudou, A. *Le Mercure en Amazonie: Rôle de L'homme et de L'environnement, Risques Sanitaires*; Expertise Collégiale; IRD Éditions: Paris, France, 2001; ISBN 978-2-7099-1467-3.
81. Guédron, S.; Tisserand, D.; Garambois, S.; Spadini, L.; Molton, F.; Bounvilay, B.; Charlet, L.; Polya, D.A. Baseline Investigation of (Methyl)Mercury in Waters, Soils, Sediments and Key Foodstuffs in the Lower Mekong Basin: The Rapidly Developing City of Vientiane (Lao PDR). *J. Geochem. Explor.* **2014**, *143*, 96–102. [CrossRef]
82. Bhardwaj, V.; Singh, D.S.; Singh, A.K. Hydrogeochemistry of Groundwater and Anthropogenic Control over Dolomitization Reactions in Alluvial Sediments of the Deoria District: Ganga Plain, India. *Environ. Earth Sci.* **2010**, *59*, 1099–1109. [CrossRef]
83. Das, A. Multivariate Statistical Approach for the Assessment of Water Quality of Mahanadi Basin, Odisha. *Mater. Today Proc.* **2022**, *65*, A1–A11. [CrossRef]
84. Miyittah, M.K.; Tulashie, S.K.; Tsyawo, F.W.; Sarfo, J.K.; Darko, A.A. Assessment of Surface Water Quality Status of the Aby Lagoon System in the Western Region of Ghana. *Heliyon* **2020**, *6*, e04466. [CrossRef]
85. Lienou, G. Impacts de la Variabilité Climatique sur les Ressources en eau et les Transports de Matières en Suspension de Quelques Bassins Versants Représentatifs au Cameroun. Ph.D. Thesis, Université de Yaoundé I, Yaoundé, Cameroon, 2007.
86. Ullrich, S.M.; Ilyushchenko, M.A.; Uskov, G.A.; Tanton, T.W. Mercury Distribution and Transport in a Contaminated River System in Kazakhstan and Associated Impacts on Aquatic Biota. *Appl. Geochem.* **2007**, *22*, 2706–2734. [CrossRef]
87. De Miguel, E.; Iribarren, I.; Chacón, E.; Ordoñez, A.; Charlesworth, S. Risk-Based Evaluation of the Exposure of Children to Trace Elements in Playgrounds in Madrid (Spain). *Chemosphere* **2007**, *66*, 505–513. [CrossRef] [PubMed]
88. Xiao, J.; Wang, L.; Deng, L.; Jin, Z. Characteristics, Sources, Water Quality and Health Risk Assessment of Trace Elements in River Water and Well Water in the Chinese Loess Plateau. *Sci. Total Environ.* **2019**, *650*, 2004–2012. [CrossRef] [PubMed]